Bio-inspired deposition of electrochemically exfoliated graphene layers for electrical resistance heating applications

NANO EXPRESS

PAPER

Bio-inspired deposition of electrochemically exfoliated graphene layers for electrical resistance heating applications

Toni Utech[1], **Petra Pötschke**[1], **Frank Simon**[1], **Andreas Janke**[1], **Hannes Kettner**[1], **Maria Paiva**[2] and **Cordelia Zimmerer**[1]

[1] Leibniz-Institut für Polymerforschung Dresden e.V. (IPF), Hohe Straße 6, D-01069 Dresden, Germany
[2] Instituto de Polímeros e Compósitos (IPC), Universidade do Minho, 4804-533 Guimarães, Portugal

E-mail: zimmerer@ipfdd.de

Keywords: electrochemically exfoliated graphene, electrical conductivity, surface resistance, dopamine, poly(dopamine), transparency, Joule-Heating

OPEN ACCESS

RECEIVED
1 September 2020

REVISED
12 November 2020

ACCEPTED FOR PUBLICATION
25 November 2020

PUBLISHED
4 December 2020

Abstract

Electrochemically exfoliated graphene (eeG) layers possess a variety of potential applications, e.g. as susceptor material for contactless induction heating in dynamic electro-magnetic fields, and as flexible and transparent electrode or resistivity heating elements. Spray coating of eeG dispersions was investigated in detail as a simple and fast method to deposit both, thin conducting layers and ring structures on polycarbonate substrates. The spray coating process was examined by systematic variation of dispersion concentration and volume applied to heated substrates. Properties of the obtained layers were characterized by UV-VIS spectroscopy, SEM and Confocal Scanning Microscopy. Electrical conductivity of eeG ring structures was measured using micro-four-point measurements. Modification of eeG with poly(dopamine) and post-thermal treatment yields in the reduction of the oxidized graphene proportion, an increase in electrical conductivity, and mechanical stabilization of the deposited thin layers. The chemical composition of modified eeG layer was analyzed via x-ray photoelectron spectroscopy pointing to the reductive behavior of poly(dopamine). Application oriented experiments demonstrate the direct electric current heating (Joule-Heating) effect of spray-coated eeG layers.

1. Introduction

Allotropes of carbon have not only played a role in the development of new materials but have also been used in consumables for several decades. Soot suspended in water with a little gum arabic as a binder made it possible to record human culture and things of everyday life 5000 years ago. In phonograph and vinyl records, soot enabled the permanent recording of music and voices. When incorporated in tires, it is essential for our mobility. With the discovery of new allotropes, mainly the nanoparticulate fullerenes and the carbon nanotubes, there were new opportunities to develop multifunctional composite materials. In the case of polymer materials, this meant the implementation of the exceptional properties of the carbonaceous nanoparticles into polymer matrixes to equip the corresponding composite material with some of the advantageous properties of the embedded nanoparticles. The aim was to adapt polymers for new applications that resulted from the desired performance properties of consumer goods. Such as tailor-made polymer materials should combine high mechanical stability and good electrical conductivity while e.g. maintaining the polymer's transparency. The desire to achieve high electrical conductivity in transparent plastics in particular is still a challenge today. The main problems, which are still unsolved, are the conversion of the orchestrated carbonaceous nanoparticles into individual particles, the prevention of their agglomeration during processing and the maintenance of their distribution in the polymer matrix over long periods of time. Since the fundamental works by Boehm [1] and the discovery of single graphene layers by Novoselov*et al* [2], graphene has increasingly attracted the interest of science [3] because of its exceptional mechanical [4] and electrical properties [5]. In 1947, Wallace predicted the excellent electrical

conductivity of two-dimensional (2D) graphene crystals [6], which based on the lack of a band gap between the valence and conduction bands. The width of the band gap can be controlled by dopants or by the architecture of the (interlayer)layer built-up [7]. The electrical conductivity is accompanied by a high thermal conductivity so that the empirical Wiedemann–Franz law, which were found for metals, broken under certain conditions [8]. Measurements of the intrinsic breaking strength of free-standing monolayer graphene corresponded to a value of 130 GPa showing the extraordinarily high strength of graphene [9]. In contrast, the van der Waals forces between individual layers assembled in a stack are weak. Novoselov *et al* demonstrated it through their exfoliation experiments with a simple adhesive tape [2]. Today, one of the major challenges for the application of graphene in materials science is its large-scale production at a low cost [10, 11]. Only an effective and efficient synthesis of individual graphene sheets guarantees the excellent properties that can improve the quality of consumer goods. So, they play a major role in photoelectric devices [12], electrically conductive transparent films, and heaters [13, 14]. Recently, graphene was applied to fabricate electrodes for retinal prosthesis [15].

Despite the interest of the industry, the inexpensive, and scalable production of graphene in reliably good quality has turned out to be a serious topic [5]. Only the question of a suitable and environmentally friendly upscale, out of the laboratory scale, remains unanswered. Different scientific methods either had a cumbersome or environmentally harmful up-scale, for example the use of aggressive, harmful or even toxic organic solvents and strong surfactants, to produce graphene and its composites. The manufacturing processes can be classified as top-down and bottom-up approaches [16, 17]. The bottom-up approach includes all high-temperature techniques, epitaxial growth, and plasma-supported vapor depositions. The top-down approach appearing to be more interesting for scalable production includes low-temperature techniques, such as electrochemical exfoliation [18, 19], and reduction of graphene oxide (rGO) [20, 21].

Dispersions of electrochemically exfoliated graphene (eeG) in water or aqueous solutions opened the opportunity to apply graphene by simple techniques such as digital inkjet printing [22], water or solvent transfer printing [23], spray coating [24, 25] and aerosol-jet (micro)printing [26]. Since the carbonaceous materials are highly hydrophobic, dispersants, such as surfactants or amphiphilic polymers are needed to suspend them in the aqueous phase. Such additional substances, however, do not have advantageous properties for the formation of dense and well-ordered graphene layers or for electrical conductivity. To improve the electrical properties, Lohe *et al* employed an electrically conductive polyaniline polymer (PANi) endowed with sulfonic acid groups guaranteeing the stability of aqueous eeG suspensions [19, 27]. The application of such novel, water dispersible eeG with straightforward spraying methods, which do not require any kinds of additional surfactants and can be processed without hesitation, appears simple and is almost independent of the substrate material and its geometry.

The modification of graphene layers by dopamine (DA) or polydopamine (PDA) has been investigated in many ways [28]. The bio-inspired modification leads to an adaptation of special graphene properties. Dopamine is a major component of adhesives that enables e.g. blue mussels (*Mytilus edulis*) to adhere to wet natural or artificial substrates in order to withstand sea waves in the coastal zone. In the presence of an oxidizing agent, dopamine is oxidatively polymerized to poly(dopamine) (PDA) [29]. Because of the self-polymerization of DA, which is the fundamental step for the extraordinary adhesive properties of PDA, both have become the subject of research in surface chemistry [28]. For example, PDA was used as an oxidizing agent for the reduction of graphene oxide [30–32], as an adhesive promoter [33, 34], or as flame retardant [35, 36]. Through preliminary work [21] we were aware of these positive properties of the bio-inspired polydopamine and applied it under specific influences.

In this work, beneficial properties of PDA have been considered to influence and tailor the electrical properties of eeG structures. We used the adhesion promoting properties of PDA to stabilize and solidify the sprayed eeG layers. The reductive properties of DA [21, 37] were used to develop a novel route to improve the electrical conductivity of the eeG layer. The work is focused on tailored eeG layers that can be used as transparent, thin layered heaters in high magnetic fields [38, 39].

2. Materials and methods

2.1. Materials

Ethanol 99% denatured with butan-2-one, propan-2-ol 98%, and *N*-Benzyl-2-(2,6-dimethylanilino)-*N*,*N*-diethyl-2-oxoethan-1-aminium benzoate (Bitrex®, min. 98.8%) were purchased from CHEMSOLUTE® (Th. Geyer GmbH, Renningen, Germany). Hydrochloric acid in propan-2-ol was obtained from Merck KGaA (Darmstadt, Germany). Polycarbonate (PC) (Makrolon® LED2245) was acquired from Covestro AG (Leverkusen, Germany). Chloroform (extra pure, 99+%, stabilized with ethanol) was purchased by Acros Organics™ (Fair Lawn, NJ, USA). Tris(hydroxymethyl) aminomethane (Trizma® base, $\geqslant$ 99.9%) was bought from SIGMA® Life Science (St. Louis, MO, USA). Dopamine hydrochloride (4-(2-aminoethyl)benzen-1,2-diol

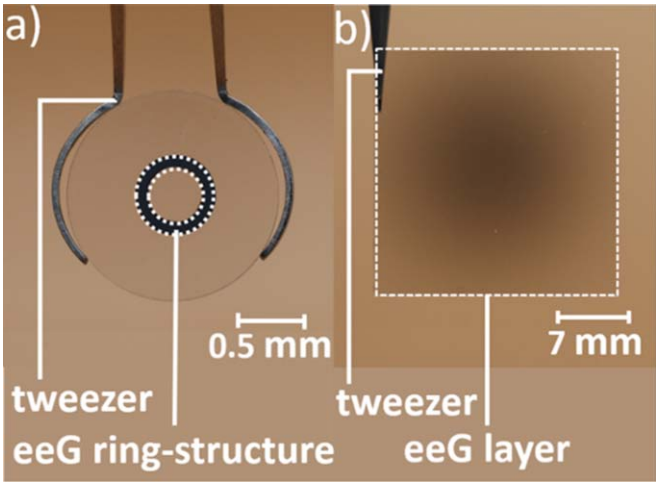

Figure 1. Spray-coated eeG as (a) ring-structure and (b) layer, both applied on a thin film of PC on top of glass-substrates.

99%) (DA) was purchased from Alfa Aesar (Ward Hill, MA, USA). E-Graphene dispersion (G-DISP-H_2O-CSO-1.6), a water-dispersible, functionalized electrochemically exfoliated graphene (eeG) was provided by Sixonia Tech GmbH (Dresden, Germany), with a concentration of 1.6 mg ml^{-1} eeG dispersed in deionized water. The Technical Data Sheet (TDS) shows that individual eeG flakes are about 1–2 μm in plane size (lateral) and about 1–5 atomic layers in thickness as assessed by SEM and AFM and assign an electrical conductivity of the material of >400 s cm^{-1}. Spectroscopic Raman specification gave D/G-band ratio of 0.1–0.2.

2.2. Thin film polycarbonate substrate preparation

A thin layer of PC was used as deposition layer for eeG. Therefore, 10 g l^{-1} PC was dissolved in chloroform. Impurities and undissolved particles were removed from the solution by filtration with a 0.45 μm PTFE syringe filter Rotilabo® from Carl Roth GmbH & Co. (Karlsruhe, Germany). The dissolved PC was processed via spin-coating using a Spin-Coater WS-650-23 from Laurell Technologies Corporation (North Wales, PA, USA). The PC solution was applied on top of cover glasses with the dimension 24 mm × 24 mm from Thermo Fisher Scientific (Waltham, Germany) to form a thin layer in four spin-coating steps. The first 3 s of each spin coating process was carried out with a velocity of 100 rpm followed by 6 s with 1600 rpm, 10 s with 1800 rpm and 15 s with 3000 rpm. The acceleration in all steps was 1000 rpm s^{-1}.

2.3. Preparation of eeG dispersions

The eeG stock dispersion (1.6 mg ml^{-1} in water) was homogenized for 1 h in an ultrasonic bath (UB) (USC-series, VWR International, Radnor, PA, USA), at 0 °C. The homogenized dispersion was diluted in ethanol to yield 0.25 mg ml^{-1} and 0.0625 mg ml^{-1}. Both dispersions were homogenized in an UB at 0 °C for 30 min.

2.4. Deposition of eeG layers

To form eeG layers, a glass substrate with a spin-coated PC layer on top was placed on a heating plate, MR 3002 from Heidolph Instruments GmbH & Co.KG (Schwabach, Germany), at a temperature of 150 °C. An airbrush pistol (AP) was used to spray the eeG dispersion. The AP was fixed at a laboratory stand with a clamp to spray vertically on top of the substrate at a working distance of 10 cm. To fill required eeG dispersion into the air channel, the specific spray volume was pipetted by using a 3.5 ml transfer pipette. The handle for controlled output of compressed air was pressed and spray impulses were created by pipetting the dispersion in batches. The impulse frequency was manually constrained in such a way that the solvent of the impinging dispersion evaporated immediately. Since in section 2.3 no filtration of the eeG-dispersion was performed, sprayed eeG layers contain all species from eeG-dispersion: remaining flakes, agglomerates of different sizes, and eeG sheets.

2.5. Preparation of eeG ring-structures

For the development of eeG ring-structures (RS) and layers the eeG dispersions were spray-coated as described before. The different eeG structures can be seen in figure 1.

The eeG RS have an external diameter of 6 mm and a width of 1 mm using special glass substrates of circular shape with a diameter of 16 ± 0.05 mm and a height of 1 ± 0.05 cm manufactured by Glaser GmbH (Dresden,

Germany). This was done in combination with two metal sheets which masked the PC layer for spray-coating to shape and create the eeG RS. One metal sheet was used as an aperture with a diameter of 6 mm and the second was a 4 mm round doted spacer.

2.6. Preparation of eeG/Dopamine dispersion

DA, 2 g l^{-1}, was added in different ratios to form 0.25 mg ml^{-1} eeG dispersion. The described mixture of DA and eeG was homogenized in an UB at 0 °C for 30 min and named as eeG/DA dispersion.

2.7. Preparation of aqueous TRIS buffer for the polydopamine coating

The aqueous TRIS buffer has been prepared from 10 mM l^{-1} Trizma® dissolved in deionized water. Drops of concentrated hydrochloric acid were added under stirring to adjust pH to 8.5.

2.8. Annealing, polydopamine coating and rinsing as post-treatment procedures

2.8.1. Annealing

Each spray-coated sample, eeG ring structure or eeG layer structure on PC layer on top of glass substrate, was annealed in a drying furnace, VT 6025 from Thermo Fisher Scientific (Waltham, MA, USA). The samples were put in the furnace at 100 °C and treated for 150 min in air at atmospheric pressure. After that the samples were taken out and cooled down to room temperature.

2.8.2. Coating poly(dopamine) on eeG RS

To deposit PDA on spray-coated eeG RS, 2 g/l of DA was dissolved in TRIS buffer at 60 °C for 30 min to polymerize DA to PDA. Afterwards spray-coated eeG RS were fixated in a holder within the PDA bath and rotated at 30 rpm for 30 min. Afterwards, eeG RS were removed from the PDA bath and rinsed with different volumes of deionized water. Finally, PDA coated eeG RS were annealed as described before.

For comparison, PDA films were spray coated directly on the PC substrate and treated in the same way.

2.8.3. Dopamine-hydrochloride modified spray-dispersion and post-treatment

As described in section 2.6, ring-structures were spray-coated with a DA modified eeG dispersion. EeG/DA RS were treated with water and annealed afterwards. The samples were washed with 100 ml deionized water or immersed by swiveling in a water bath for 120 min. EeG/DA RS were annealed as described before.

2.9. Characterization methods

2.9.1. Thickness determination of eeG RS

The thicknesses of the eeG RS were measured with confocal microscope MarSurf CM expert from NanoFocus AG (Oberhausen, Germany). The NanoFocus AG objective was used with a 1600 μm image field length at a short working distance and a 10-fold magnification and a numerical aperture of 0.30. At an exposure time of 60 ms, a measurement field of 7.488 $\times$ 7.488 mm^2 and a pitch segmentation of 0.931 μm, and a Fast-3D-evaluation algorithm was applied. The provided 3D model was analyzed with μsoft metrology from NanoFocus AG (Oberhausen, Germany).

For each sample, four cross sections were analyzed at a 90° angle to each other. An average eeG thickness was calculated based on the thicknesses of the individual cross-sections.

2.9.2. AFM measurement

Since confocal microscopy cannot determine the thickness of highly transparent layers, atomic force microscopy (AFM) was applied to measure very thin eeG layers. The instrument Dimension Fast Scan (Bruker-Nano, Billerica, MA, USA) recorded in tapping mode. The used AFM tip was a Tap 300 (Budget Sensors, Sofia, Bulgaria) with a tip radius of 10 nm, a spring constant of 40 N m^{-1}, and a resonance frequency of 300 kHz. The NanoScope Analysis 2.0 software (Bruker-Nano) was used for evaluation. For the layer thickness analysis, a scratch was made on the entire sample using a razor blade. Since the sample surface consists of areas with pristine PC and the composite PC/eeG, the eeG thicknesses were calculated by subtraction of the measured thicknesses of PC.

2.9.3. Electrical resistance measurement

The electrical volume resistance of eeG RS was measured by the four-point method with a micro-pin-measuring-unit built at the IPF. The unit was used in combination with the Keithley DMM2001 multimeter from Tektronix (Beaverton, OR, USA). The electrical volume resistance is calculated and displayed in DM2001 by means of ohmic law. In order to eliminate line and transition resistances in measuring objects with a low

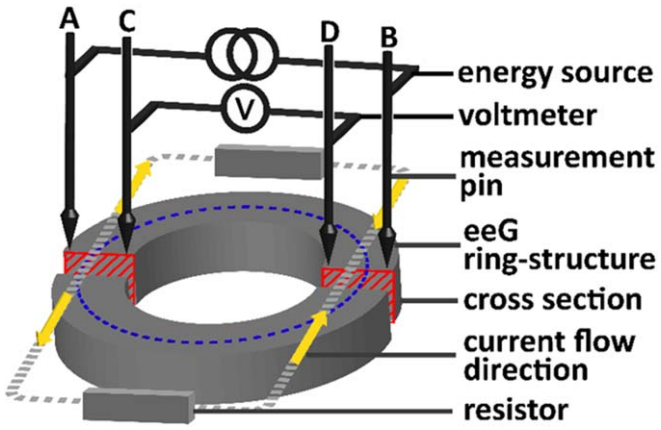

Figure 2. Schematic illustration of the measuring principle and the half-ring resistance network and the mean path as blue dotted line.

resistance value, the 4-wire measuring technique was used, i.e. the constant current supply and the voltage measurement are carried out via separate lines.

In order to determine the electrical volume resistance of the eeG RS, one would actually have to cut the ring at one point. But this would result in destroying the structure. A non-destructive measurement is possible, however, if the measuring pins are arranged opposite to each other. Two half rings are then measured in parallel. Assuming a homogeneous structure, the mean ring resistance $\bar{R}$ is calculated from the measured resistance value R_i as equation (1) describes:

$$\bar{R} = \frac{1}{n}\sum_{i=1}^{n}(4 \cdot R_i) \tag{1}$$

where $\bar{R}$ is the mean resistance per sample, R_i is the measured ring resistance per single measurement and n is the number of measurements per sample. Each measured R_i value was multiplied by the factor four which derived from the used ring geometry and pin arrangement. Within the described measuring setup, a whole eeG RS acts as slit in two half rings, which are treated like two parallel connected resistors. This is illustrated in figure 2.

2.9.4. Electrical conductivity of eeG RS

In order to calculate the electrical conductivity σ, the electrical resistivity ρ was calculated first due to the reciprocal dependency between σ and ρ, equation (2).

$$\rho = \frac{1}{\sigma} \tag{2}$$

The electrical resistivity of the volume of eeG RS was calculated by equation (3):

$$\rho = \bar{R} \cdot \frac{A}{l} \tag{3}$$

where ρ represents the electrical resistivity, which is calculated with the mean electrical resistance $\bar{R}$ of the measured volume of the eeG RS, the cross-section A (marked in figure 2 as red areas) and the mean path length l (marked in figure 2 as blue dotted line) which was simplified as the mean arc length of the eeG RS with a circumference of 15.71 mm. The calculation of the cross-section A is described in equation (4).

$$A = w \cdot h \tag{4}$$

where w is the width and h the height of the eeG RS. The only variable is the height h, since the width w is fixed at 1 mm.

2.9.5. SEM characterization

Samples were analyzed with the scanning electron microscope SEM Gemini Neon 40 EsB from Carl Zeiss Microscopy GmbH (Oberkochen, Germany) with a secondary electron (SE2)- and an InLens-detector. Samples were mounted on metal stubs using a sticky carbon strip for fixation. Samples were coated with 3 nm of platinum to avoid electrostatic charging of sample surfaces.

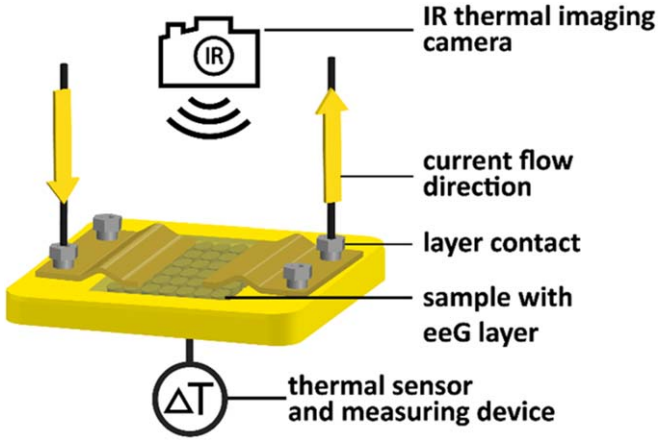

Figure 3. Schematic setup for Joule-Heating experiments.

2.9.6. X-Ray photoelectron spectroscopy

All x-ray photoelectron spectroscopy (XPS) studies were carried out by means of an Axis Ultra photoelectron spectrometer (Kratos Analytical, Manchester, UK). The spectrometer was equipped with a monochromatic Al Kα ($h \cdot \nu = 1486.6$ eV) x-ray source of 300 W at 15 kV. The kinetic energy of photoelectrons were determined with hemispheric analyzer set to pass energy of 160 eV for wide-scan spectra and 20 eV for high-resolution spectra.

Samples of differently treated eeG layers were prepared as sprayed films on microscope cover plates (22 mm × 22 mm, Bresser GmbH, Rhede, Germany). The eeG coated cover plates were mounted on a sample holder enabling the samples transport in the recipient of the XPS spectrometer.

During all measurements, electrostatic charging of the sample was avoided by using a low-energy electron source working in combination with a magnetic immersion lens. Later, all recorded peaks were shifted by the same value that was necessary to set the C 1s peak to the reference binding energy of 283.99 eV. This reference value was determined from XPS spectra from a carbon nanotube-filled poly(lactic acid) composites [40].

Quantitative elemental compositions were determined from peak areas using experimentally determined sensitivity factors and the spectrometer transmission function. Spectrum background was subtracted according to Shirley [41]. The high-resolution spectra were deconvoluted by means of the Kratos spectra deconvolution software. Free parameters of component peaks were their binding energy (BE), height, full width at half maximum and the Gaussian-Lorentzian ratio.

2.9.7. Optical transmittance of eeG layers

The transparency analysis of eeG layers were performed by UV/VIS spectroscopy using a Cary 60 UV-Vis spectrometer from Agilent Technologies Inc. (Santa Clara, CA, USA) within the wavelength range of 200 to 800 nm and using a scan rate of 300 nm min^{-1}.

2.9.8. Joule-Heating of eeG layers

The Joule-Heating of samples with eeG layers were examined in a special measuring unit built at the IPF, see figure 3. Two metal slides were screwed down on the eeG layer. Both contacts, each metal sheet is 15 mm in length, were placed at a distance of 18 mm. Connected to the power supply, the Keithley DM2001 multimeter was connected in series to measure the current. A thermal sensor was placed underneath the sample. The generated heat was recorded with a Voltcraft 302/J thermometer and in addition to the FLIR i7 thermal camera from FLIR® Systems Inc. (Wilsonville, OR, USA). The applied voltage was manually increased in the intervals of 1 V, 2 V, 5 V, 10 V, 15 V, 20 V and 30 V. The temperature was measured at time intervals of 1 min, 2 min, 5 min, 10 min, 15 min, 20 min, and 30 min. The applied electrical voltage was maintained over time intervals. After reaching each respective time interval, the temperature was measured and the electrical voltage was regulated to the next set-point.

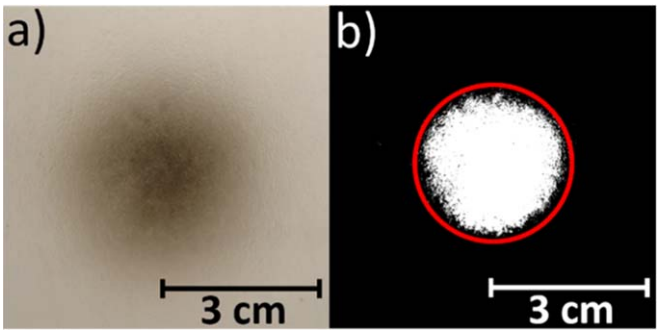

Figure 4. Photo of spray-coated eeG (a) and converted into (b) a binary image to spot the area of impact.

Table 1. Resulting masses of spray-coated eeG layers and ring-structures.

Sprayed volume [ml]	eeG concentration [mg/ml]	Sprayed eeG mass [μg]	
		ring-structure (2% of AOI)	layer (80% of AOI)
1	0.0625	1	50
2		3	100
1	0.25	6	200
3		20	600
6		30	1200
8		40	1600

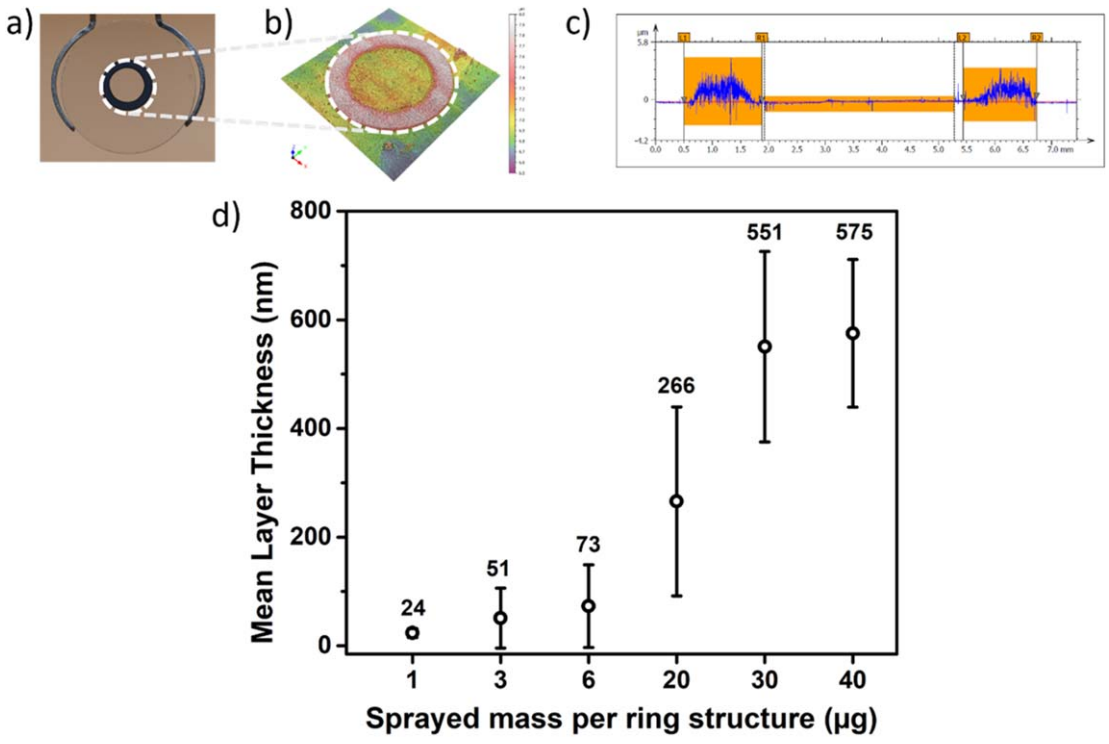

Figure 5. Overview of thickness determination method using confocal microscopy for eeG RS, (a) sprayed eeG RS on a round, tweezer fixed, glass-PC substrate, (b) the corresponding 3D model, (c) image cross section to be used for height estimation and mean value calculation, and (d) Mean Thickness and Standard Deviation of eeG RS in dependence of sprayed eeG mass.

Table 2. Mean layer thicknesses and standard deviations for spray-coated eeG RS.

Method	AFM	Confocal microscopy				
Spray-coated eeG mass [μg]	1	3	6	20	30	40
Mean Layer Thickness [nm]	24	51	73	266	551	575
Absolute Standard Deviation [nm]	± 8	± 55	± 76	± 174	± 175	± 136
Relative Standard Deviation [%]	34	110	105	65	32	24

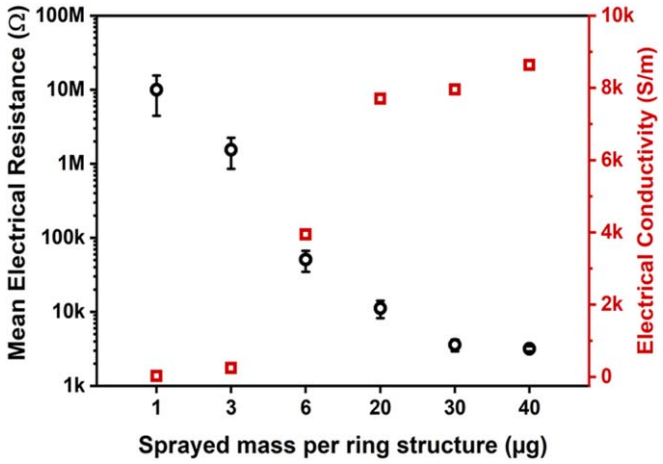

Figure 6. Mean Electrical Resistance and Electrical Conductivity of spray-coated eeG RS with different deposited eeG quantities.

3. Results

3.1. Calculation and standardization of the adhering spray-coated eeG mass

To determine the spatial distribution of the eeG sheets and particles on the spray-coated substrates, the size of the surface to which the largest part of the eeG adheres was determined. Figure 4(a) shows a top-view photograph of a spray-coated area. The spray-coating parameters are mentioned in section 2.4. In addition, 6 ml of a 0.25 mg ml^{-1} eeG dispersion was used to develop the discernible area of impact (AoI). After the proper threshold setting, the software ImageJ (Wayne Rasband, National Institute of Health, Bethesda, MD, USA) was used to convert the photograph into a binary image to obtain the AoI, as shown in figure 4(b), inside the red circle. Under the selected spray-coating conditions, this AoI was determined to be 7.07 cm^2 in size, with a diameter of 3 cm. It is assumed that most eeG sheets and particles adhere to this AoI. With this limited area the mass of adherent eeG per sprayed dispersion volume can be approximated by subtracting the measured area due to the given substrate geometries of eeG layer and ring-structure in sections 2.2 and 2.5. As a result, the area of the eeG layer is about 80% of the AoI. Regarding the area of the eeG RS, only approx. 2% of the layer AoI was spray-coated.

The used spray-coating eeG dispersion volumes, concentrations, and resulting eeG masses for the layers and ring-structures are listed in table 1.

3.2. EeG RS and thickness determination

The thickness measurement by confocal microscopy was supported by rendering 3D models (figures 5(b) and (c)). The standard deviations of the eeG RS measured with AFM and confocal microscopy differ. Figure 5(d) shows the measured thicknesses with both the methods. It can be seen that the measured structure thickness and the associated standard deviation increase with increasing sprayed mass of eeG. The lowest structure thickness is about 22 nm and the highest about 605 nm. The absolute standard deviation raises with increasing sprayed eeG quantity. The only exception is seen when eeG RS was spray-coated with 40μg, suggesting that the eeG sheets and particles are not only planarly inhomogeneous Gaussian distributed [42], but also the eeG particles are disorderly superimposed in height, as it was seen in the work of Nasim *et al* [43]. The values are summarized in table 2.

3.3. Electrical properties of spray-coated eeG RS

To use structures as a susceptor in a high magnetic field application or as a thermally conductive layer for Joule-Heating, it is important to reproducibly manage the electrical material characteristics of the sprayed eeG RS or

Table 3. The mean electrical resistances, conductivities and their standard deviations for spray-coated eeG RS.

Spray-Coated eeG mass [μg]	Mean electrical resistance and standard deviation [kΩ]	Electrical conductivity [S/m]
1	10000 $\pm$ 554	27
3	2000 $\pm$ 692	245
6	51 $\pm$ 16	3900
20	11 $\pm$ 3	7700
30	4 $\pm$ 0.7	8000
40	3 $\pm$ 0.3	8600

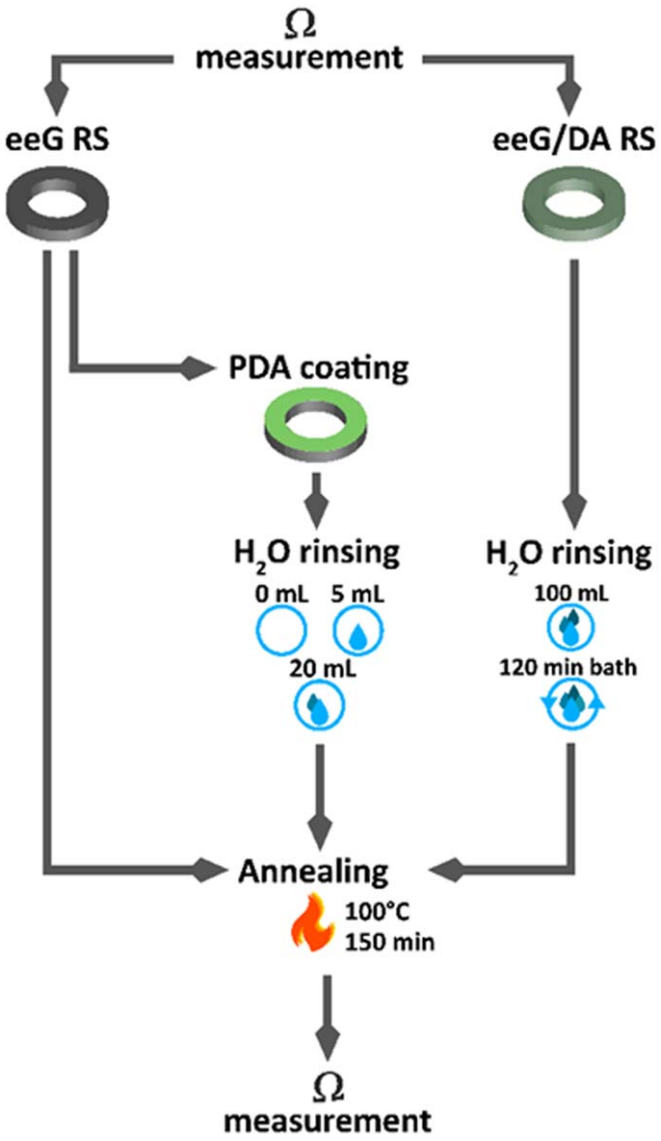

Figure 7. Overview of the different eeG RS and eeG/DA RS treatments routes.

eeG layers. Electrical conductivity was estimated with the determined values of the eeG thickness and the electrical resistance measurements.

The dependencies of heat generated by a dynamic magnetic flux and induction phenomenon or by Joule-Heating are based on the same physical laws and can be described by equation (5).

$$E = \frac{U_{(t)}{}^2}{R} \tag{5}$$

Table 4. Overview of the four different treatments to increase eeG RS electrical conductivity.

Spray-coated RS	Ap-proach	PDA coating	Rin-sing	Immer-sion	Annea-ling
eeG	1	☒	☒	☒	☑
	2	☑	☑	☒	☑
eeG/DA	3	☒	☑	☒	☑
	4	☒	☒	☑	☑

E is energy generated by an applied or induced voltage U and R is the electrical resistance. With a decrease in electrical resistance the generated energy increases while the electrical voltage remains constant. For optimum energy conversion, the electrical resistance should be as low as possible and, vice versa, the associated electrical conductivity of the eeG RS should be as high as possible. The highest achievable electrical

conductivity is a material-dependent constant and, according to TDS given to > 400 s cm^{-1} for the eeG material [44].

To determine the electrical resistances of the eeG RS a measuring unit was developed to contact the eeG RS and evaluate the electrical resistance at room temperature, as shown in figure 2. Figure 6 shows the mean values of electrical resistances for the eeG RS. With increasing mass of the sprayed eeG the electrical resistance decreases from around 10 ± 0.6 MΩ to 3 ± 0.2 kΩ. With the related layer thicknesses (compare figure 5), the electrical conductivities were calculated, see red data points belonging to the right axis in figure 6.

The calculated electrical conductivities clearly show a sigmoidal increase, which indicates a percolation threshold between 3 and 20 μg sprayed eeG mass [45, 46]. The sprayed eeG RS with 1 and 3 μg achieved an electrical conductivity of 27 ± 18 to 245 ± 150 s m^{-1}. Doubling the sprayed eeG mass to 6 μg resulted in an approximately 16-times increase to about 3900 s m^{-1} in electrical conductivity value. The spray mass of 20 μg eeG led to the doubling of conductivity value to about 7700 s m^{-1}. A further increase of the sprayed eeG mass to 30 and 40 μg led to a marginal improvement of the electrical conductivity to 8000 s m^{-1} and 8600 s m^{-1}, respectively. Saturation of conductivity is reached at 20 μg sprayed eeG mass. Compared to the electrical conductivity given in [44] ($\sigma > 40{,}000$ s m^{-1}), our spray-coating process produced eeG RS with an electrical conductivity approx. five times lower. All measured electrical resistances and calculated electrical conductivities are listed in table 3.

The evaluated electrical properties do not reach the values which were specified in the data sheet of this material. Also, it was lower than the values reported in [44]. To increase the conductivity of the ring structures, post-treatments of the sprayed eeG RS were established while maintaining the same deposition process. The expectation was to modify the microstructure of the deposited layers in such a way that better contacts between the eeG sheets and arrangements of eeG particles would be possible and subsequently could result in higher conductivity.

3.4. Modification of eeG RS

In order to decrease the electrical resistance three different treatments were performed that influence the arrangement of the eeG sheets and particles as well as their degree of oxidization. For each treatment, see table 4, a spray volume of 6 ml eeG dispersion, either pristine eeG or eeG/DA, was used. The resulting mass of sprayed eeG will be explained individually.

EeG RS were annealed in the first treatment. In the second, eeG RS were coated with PDA and subsequently rinsed with different amounts of water and annealed afterwards. The rinse volumes in the second route were 0 ml, 5 ml and 20 ml. The third treatment route is the preparation of an eeG RS and DA mixed dispersion, which was sprayed to deposited eeG/DA RS, afterwards rinsed with different amounts of water or, immersed in water as in route four, and finally annealed. 100 ml rinse volume was used for immersion due to swiveling in a water bath for 120 min. An overview of the described routes are shown schematically in figure 7.

The individual treatments and their effect on the electrical properties are investigated and compared.

3.4.1. Approach 1 - annealing

As described by Orts *et al* [47] and Kanaya *et al* [48], thin polymer layers made by spin coating relax during annealing.

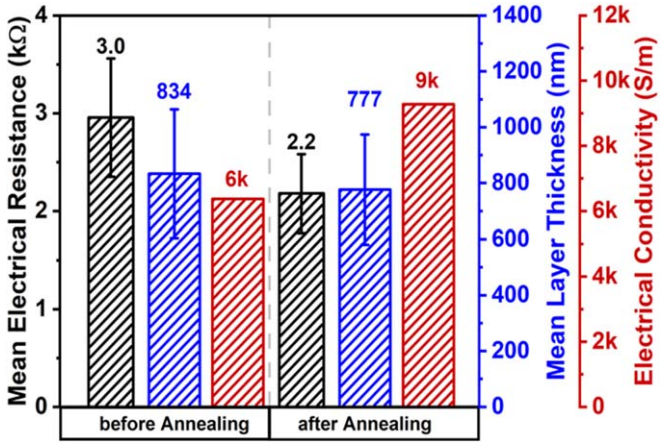

Figure 8. Mean Relative Changes of the Electrical Resistance, Layer Thickness and Electrical Conductivity after Annealing.

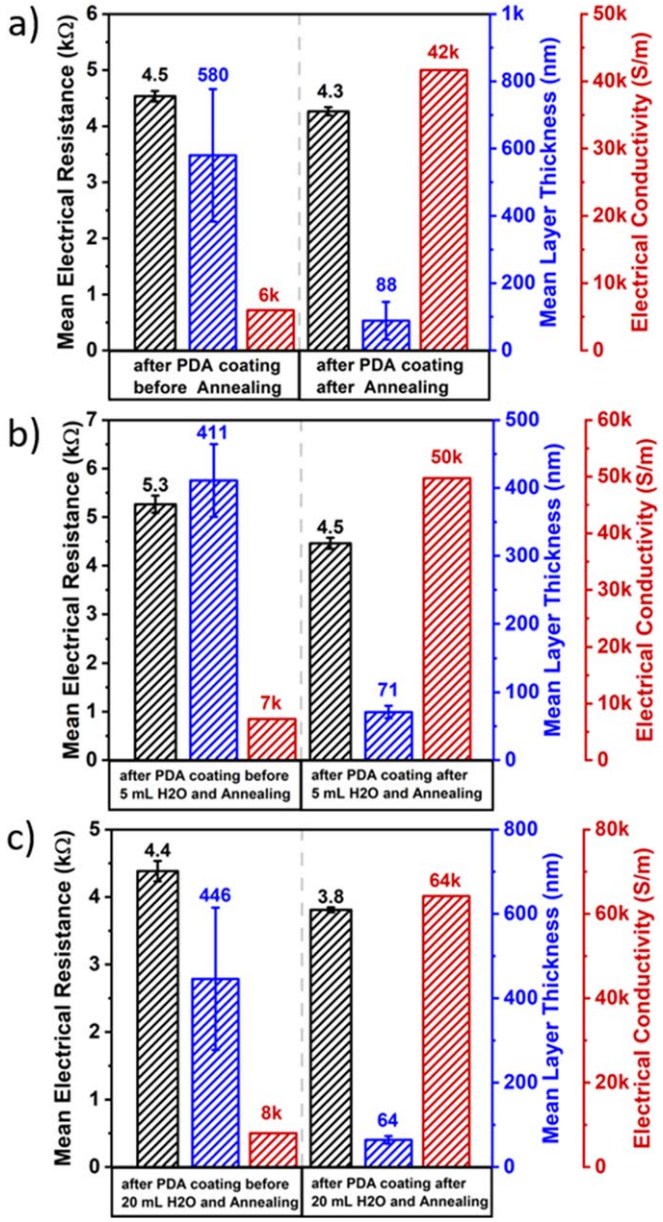

Figure 9. Mean values of the Electrical Resistances, Layer Thicknesses and Electrical Conductivities of the PDA post-treatment of eeG RS before and after rinsing with (a) 0 ml, (b) 5 ml and (c) 20 ml water and Annealing.

Due to the negative thermal expansion coefficient of polymers, contraction of the polymer with spray-coated eeG RS on top is hypothesized to influence the alignment and the connectivity of the sprayed eeG sheets and particles during a thermal treatment. Therefore, eeG RS deposited from 6 ml sprayed 0.25 mg ml^{-1} eeG dispersion was treated for 150 min at 100 °C.

Figure 8 shows the mean electrical resistances, film thicknesses and calculated electrical conductivities before and after the annealing. The value of the mean electrical resistance measurement on the eeG ring structure selected for the annealing process is 3 ± 0.6 kΩ. After annealing, this value slightly decreases to 2.2 ± 0.4 kΩ. The measured layer thickness of the eeG RS also decreases slightly, from 834 ± 230 nm to 777 ± 197 nm. The decrease of electrical resistances and layer thickness results in an increase of the electrical conductivity from 6.4 to 9.3 kS m^{-1}.

The respective relative changes X_{rel} of the described parameters were calculated as shown in equation (6) and published in [49]:

$$X_{rel} = \frac{X - X_i}{X_i} \tag{6}$$

X is general variable for a described parameter set and the index i as the initial value at the beginning of the measurement. In facts, due to the annealing the electrical resistance decreases by 26%, and the layer thickness by 6.8%, which resulted in 31% increase in electrical conductivity. This can be attributed to the escape of solvent residues [50] and the relaxation of the polymer PC layer [47, 50–52], and will be discussed further in-depth in section 4. Acik *et al* reported the evaporation of intercalated water [53].

3.4.2. Approach 2—post-treatment of eeG RS with PDA, rinsing and annealing

Annealing at elevated temperature (here 100 °C) shows a desired positive effect on the electrical conductivity of the eeG RS. To further enhance the electrical conductivity, a bio-inspired approach using PDA was investigated. Since DA is a naturally occurring compound [28], PDA is used as a bio-inspired adhesion promoter and for functionalization [28, 54]. Based on this reported application, PDA was used to cover eeG RS to mechanically stabilize and to improve the contact between the eeG sheets and particles in the layer, like remaining not exfoliated flakes and eeG agglomerates of different sizes. A first post-treatment procedure of the PDA-coated eeG RS was performed without water rinsing after PDA deposition. After annealing mean electrical resistance, layer thickness and electrical conductivity were determined, see figure 9(a). The PDA coating and the annealing led to a negligible decrease of the electrical resistance from 4.5 ± 0.09 kΩ to 4.3 ± 0.07 kΩ. The reduction of the layer thickness is approx. 492 nm, from 580 ± 197 nm to 88 ± 56 nm. Thus, both measured variations result in an increase of the electrical conductivity from approx. 6 to ~42 kS m^{-1}. The electrical resistance change is − 6%, the thickness change is −85%. This increased electrical conductivity by 595%.

To ensure that no loosely attached or adsorbed particles or molecules, e.g. DA solution components, influence the measurements, the samples were rinsed with different volumes of water as described in section 2.8.2. First, 5 ml of water was used after PDA coating. Mean electrical resistance, mean layer thickness and electrical conductivity values were monitored during the procedure as shown in 9b). The electrical resistance decreased from 5.3 ± 0.18 kΩ to 4.5 ± 0.11 kΩ. The mean thickness decreased from 411 ± 53 nm to 71 ± 9 nm. The electrical conductivity increased from 7.3 to about 50 kS m^{-1}. The corresponding relative values of electrical resistances decrease, layer thickness decrease and conductivity increase were indicated by about 15%, 83%, and 585%. Again, the significant decrease in thickness causes a strong increase in electrical conductivity.

To continuously improve the process, four times higher volume of water was used for rinsing. The results of the mean electrical resistance, layer thickness and electrical conductivity were calculated from values before and after the treatment, figure 9(c). Mean electrical resistance of 4.4 ± 0.15 kΩ were measured before coating and annealing. After the rinsing and annealing treatments, the value of 3.8 ± 0.11 kΩ was achieved. The film thickness decreased from 446 ± 170 nm to 64 ± 9 nm. The calculated electrical conductivity increased from approx. 8.03 to 64 kS m^{-1}. Summarizing the relative changes, a decrease in electrical resistance by 13% and in thickness by 86% have been observed. These data result in the largest increase in electrical conductivity by 699% in comparison with the tested PDA-treatment procedures so far.

Conductivity values of 42 kS m^{-1}, 50 kS m^{-1} and 64 kS m^{-1} were achieved with 0 ml, 5 ml, and 20 ml of rinsing volume. After PDA treatments, electrical conductivities were comparable to the given data in the TDS from the manufacturer and reported for a PDA modified fiber based on graphene by Ma *et al* [55].

In this context it was found that spray-coated PDA films did not show measurable conductivity, neither before nor after annealing. It was confirmed that the DA layer, before and after annealing, was dissolved by rinsing with bi-distilled water and thus no DA remained on the substrate. Thus, the PDA itself is not expected to contribute to the found changes.

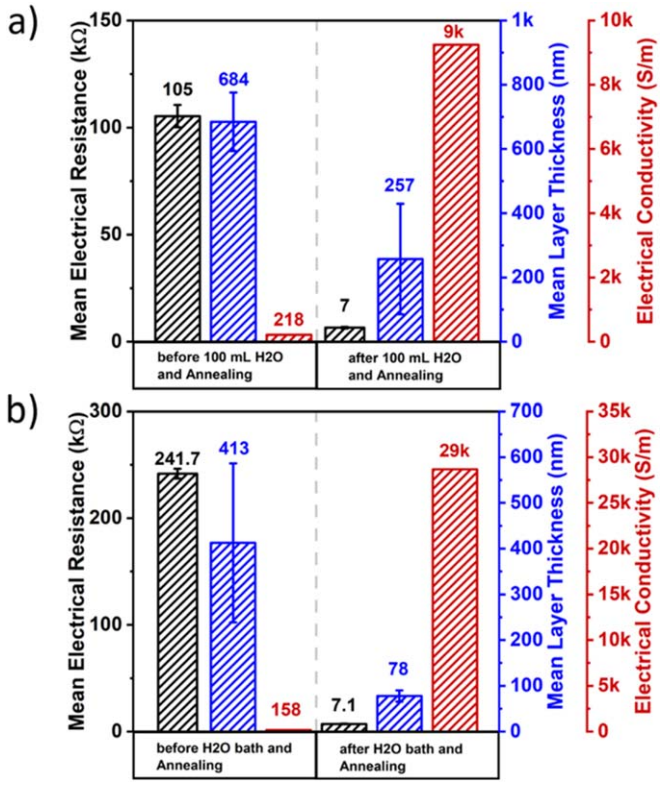

Figure 10. Mean values of the Electrical Resistances, Layer Thicknesses and Electrical Conductivities of the analysed eeG/DA RS before and after rinsing with (a) approach 3–100 ml water and Annealing and (b) approach 4 - after swivelling for 120 min in water and Annealing.

3.4.3. Approach 3 - spray-coated eeG/DA RS, rinsing and annealing

Since the procedures in the former section apply a top-layer of PDA to the eeG RS, the following investigations were performed to polymerize DA in-situ during the deposition process of eeG RS. These experiments should help to answer the questions: a) What impact the sprayed eeG/DA dispersion has on the measured electrical resistance and thickness? b) What effect can be manifested by a post-treatment with water and annealing?

The composition of eeG/DA dispersion was described in section 2.6. To deposit eeG/DA RS a volume of 6 ml of the eeG/DA dispersion was spray-coated. The eeG/DA RS were rinsed with water and annealed.

Electrical resistance and thickness of eeG/DA RS have been measured. The mean electrical resistance value of 105 $\pm$ 5 kΩ is significantly higher than for samples with PDA post-treatment. The initial mean layer thickness of 684 $\pm$ 91 nm is similar to that of the sample studied in section 3.2. After the treatment with 100 ml water and annealing, a decreased mean resistance of 7 $\pm$ 0.4 kΩ and a reduced layer thickness of 257 $\pm$ 172 nm was recorded as shown in figure 10(a). These are relative decreases of 87% and 62%. The corresponding electrical conductivity increased from 218 s m^{-1} to 9 kS m^{-1}, see figure 10(a). This represents an increase of 4000%.

The electrical resistances achieved by both treatment routes (post PDA coating or in-situ-deposition of PDA) are not directly comparable. By using 2 g/l DA mixed with a 0.25 mg ml^{-1} eeG dispersion the quantity of deposited eeG is reduced. Nevertheless, the calculated electrical conductivity is about 1.3 kS m^{-1} higher in comparison to the pristine eeG-RS in table 3, which was sprayed with an eeG mass of 20 μg and measured with an almost similar layer thickness of 266 nm.

But for all investigated procedures, PDA shows a clear decreasing effect on electrical resistances and layer thickness.

3.4.4. Approach 4 - spray-coated eeG/DA RS, immersion and annealing

The final variation of the eeG/DA RS post-treatment is immersion, due to swivel the eeG/DA RS in water for 120 min at r.t,. and to anneal it afterwards. This treatment resulted in a decrease of the mean electrical resistance from 242 $\pm$ 5 kΩ to 7 $\pm$ 0.3 kΩ. The mean layer thickness of 413 $\pm$ 174 nm decreased to 78 $\pm$ 12 nm and the electrical conductivity increased from 158 s m^{-1} to 29 kS m^{-1} as shown in figure 10(b). This corresponds to relative reductions of 97% concerning the electrical resistance, 81% for the layer thickness and an increase of electrical conductivity by 18000%.

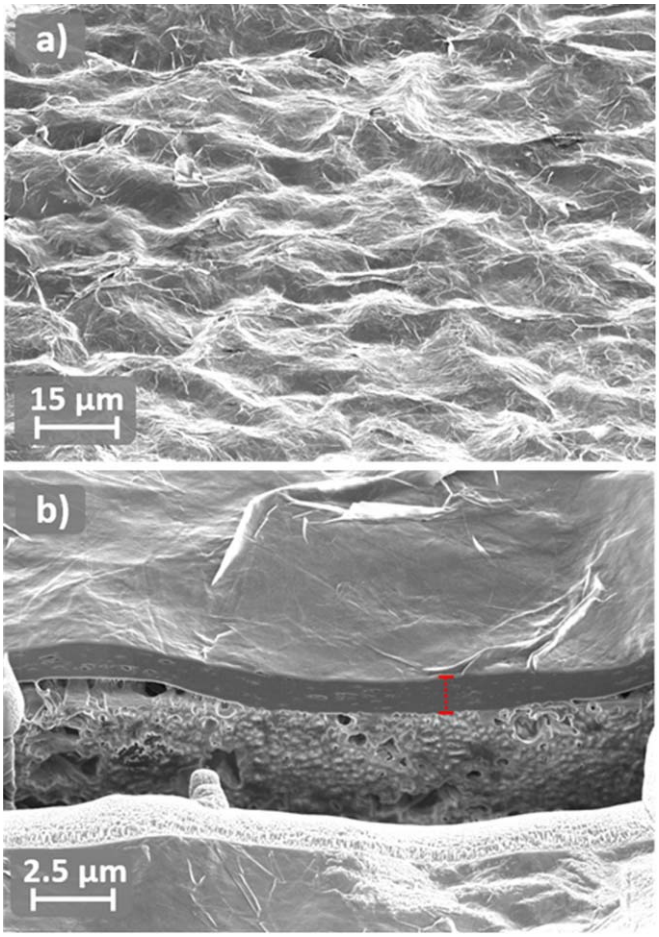

Figure 11. SEM images of (a) a pristine eeG layer and (b) a cross section of a pristine eeG layer on top of a polycarbonate membrane.

This behaviour is in contrast to the PDA post-treatment of eeG RS, see section 3.4.2, because the electrical conductivities are higher in absolute but the relative increase is lower. This shows the need for a deeper understanding and the enormous potential of such PDA treatments of eeG materials.

3.5. Structure analysis of modified eeG RS

To illustrate the differences in electrical behaviour, morphological investigations were carried out. For the analysis of the obtained results, pristine eeG RS was investigated with SEM, see figure 11. The surface of the pristine eeG layer as seen in figure 11(a) shows a rough rippled topography with a surface similar to crumpled tissue [56]. In addition to the eeG surface, figure 11(b) shows a sample cross-section. The red bar refers to the eeG layer thickness. Similar to findings by Geng *et al* on graphene and nitrogen-doped graphene [56], the SEM images show graphene sheets arranged randomly and disoriented. Similar arrangements of graphene flakes have been demonstrated by Xie *et al* [57] and Dimiev *et al* [58]. Xie *et al* also proposed that the graphene-specific surface topography is caused by the bulging of the individual flakes. Dimiev *et al* [58] were even able to illustrate the transparency of such graphene flake, which was enabled by studying different positions of individual overlaps of the analyzed graphene flakes.

Figure 12 shows the SEM images of an eeG RS post-treated with PDA (figures 12(a)–(d)), and images of an eeG/DA RS, see figures 12(e)–(h). The PDA post-treated eeG RS in figure 12(a) in which the red dotted lines mark the inner and outer contours of the eeG RS show that there is almost no difference in the appearance of the eeG RS and the underlying PC layer due to the PDA layer on top of both. At higher magnification, compare figures 12(b), (c) the agglomerates of remaining PDA particles become visible as brighter areas spread over entire surface. In figure 12(d) a rough surface is visible hosting a spherical PDA agglomerate. This phenomenon of agglomeration of PDA on graphene surfaces is confirmed by works of Pinithchaisakula *et al* [59], Li *et al* [60] and Yu *et al* [34]. Due to the PDA coating no individual eeG structures, expected to be in the lateral size of 1–2 μm, can be observed. Figure 12(e) shows an eeG/DA RS. The circle of red dotted lines implies the penetration point of one measuring pin of the resistance measurement, more clearly seen in figure 12(f).

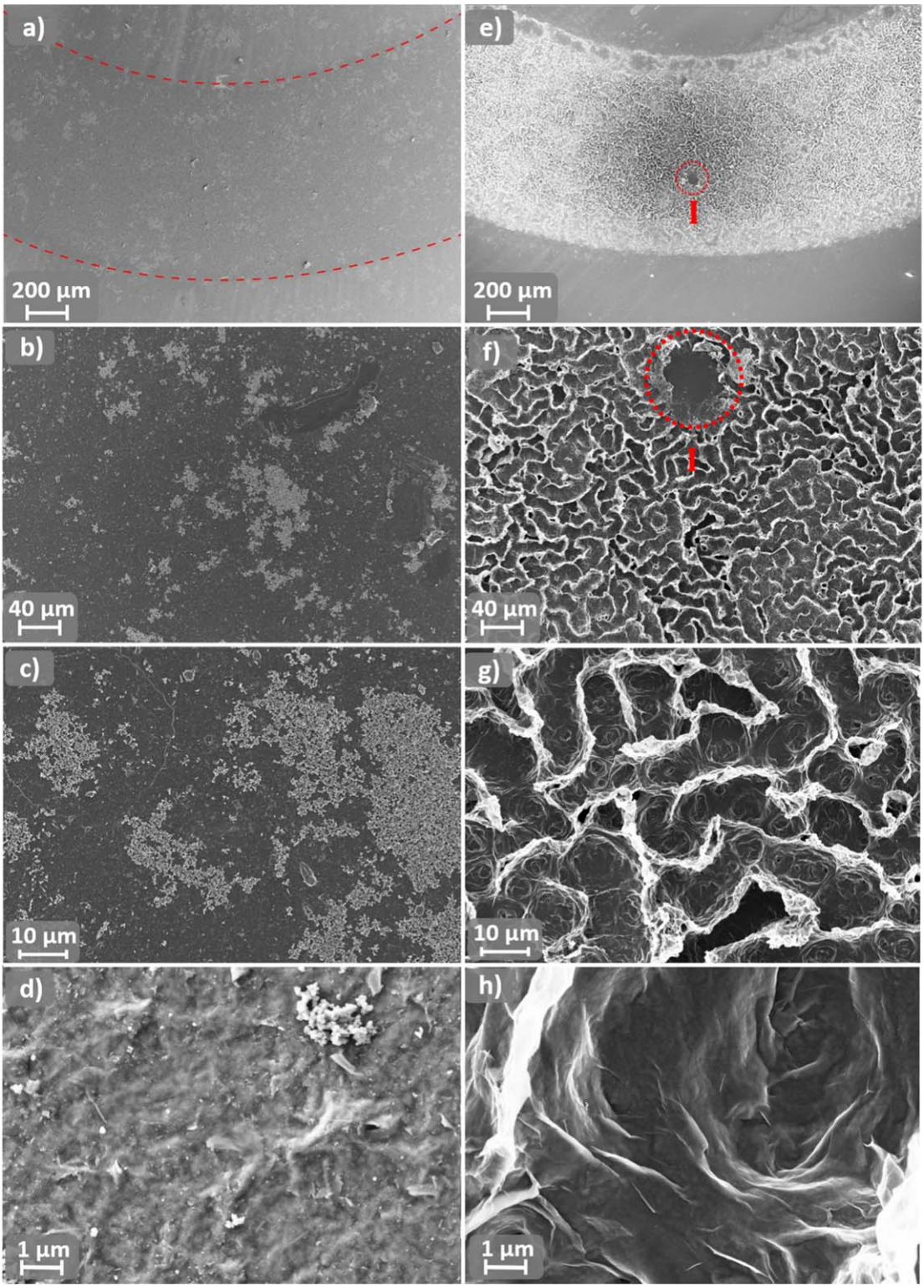

Figure 12. SEM images of eeG RS post-treated with PDA (a) to (d) and eeG/DA RS (e) to (h). All samples have been rinsed with water and annealed. Red dotted line in (a) highlights the contour of the eeG RS, in (e) and (f) the red circle marks the penetration point of the measuring pin of the resistance measurement.

Surface topography shows an unexpected phenomenon; instead of the formation of a homogeneous layer, a structure similar to meandering tubes was observed. However, the InLens SEM-image may give an incorrect impression of the structure, as the white meanders represent charged areas near the surface. Further, higher magnified images present a burr and cavities. Layer-like structures, which however appear perpendicular oriented to the sample surface are the defining eeG/DA topography. In summary, it was almost impossible to detect and verify the eeG RS sheets or flakes. With regard to the eeG/DA RS surfaces, ridge-like rises and crater-

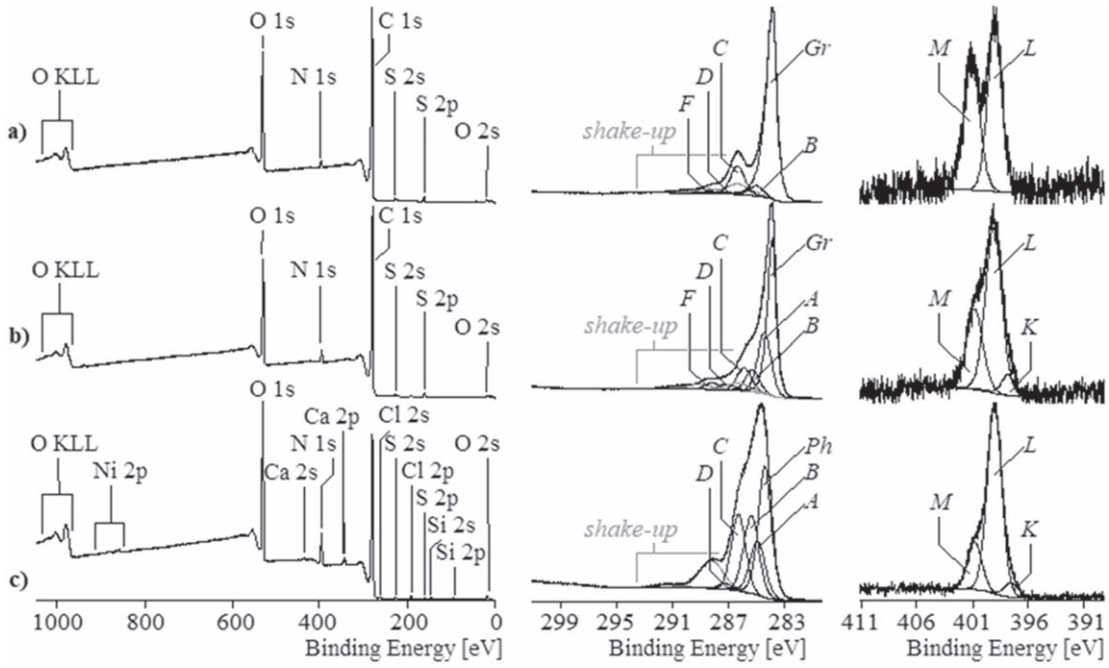

Figure 13. XPS wide-scan (left column), C 1s (middle column), and N 1s (right column) high-resolution element spectra recorded from a spray-coated film made from pristine eeG (a), a spray-coated film made from eeG with DA polymerized in suspension (b), and an eeG film, which was coated with PDA (c).

like hollows were observed. This local difference in the thickness are averaged by the measurements of the layer thickness using confocal microscopy.

3.6. X-ray photoelectron spectroscopy

XPS was applied to clarify, whether the treatment with PDA or DA is accompanied by a chemical reduction of the eeG, which might be one explanation for the decreases of electrical resistances using both PDA based procedures routes. Figure 13(a) shows XPS spectra recorded from a pristine eeG, which was sprayed on a glass substrate (microscope cover plate). The absence of the silicon Si 2p peak which is expected at 102 eV and the corresponding Si 2s peak at 154 eV, ensured that the eeG film was sufficiently thick to get only spectroscopic information from the applied eeG film. In addition to the expected C 1s peak the wide-scan spectrum also shows the presence of considerable amounts of oxygen.

Nitrogen's N 1s peak with a [N]:[C] ratio of 0.02 and Sulphur's S 2p and S 2s peaks with a [S]:[C] ratio of 0.012 resulted from a sulfonated polyaniline dispersant, which is adsorbed on the surface of the eeG particles. Ultrasonic treatment of the eeG dispersion before the spraying did not result in any significant changes in the XPS spectra. The shape of the high-resolution C 1s spectrum seemed to be characteristic of carbonaceous substances. This is shown in figure 13 in the middle column. Its tailing on the high energy side resulted from excited states of the sp^2-hybridized carbon atoms forming the graphene-like lattices. Linear combinations of two p_z orbitals result in a quasi-continuum of overlapping π and π^* orbitals.

The consumption of external energy leads to electron transitions from occupied π to unoccupied π^* orbitals. The photoionization not only ejects electrons from carbon atoms in their ground state, but also some from the excited states.

Photoelectrons of the excited states were collected as so-called *shake-up* peaks. In contrast, the main component peak *Gr* at 283.99 eV shows sp^2-hybridized carbon atoms in their ground state. The second maximum in the C 1s spectrum indicated a high number of oxygen-bonded carbon atoms. The findings are confirmed by the high relative oxygen at a [O]:[C] ratio of 0.188 found in the wide-scan spectrum. Component peak *C* arising at 286.49 eV shows preferably phenolic C–OH. The peak area remaining after the subtraction of the *shake-up* peaks and the component peaks *Gr* and *C* were deconvoluted into the component peaks *B* at 285.1 eV, *D* at 287.54 eV and *E* at 288.45 eV.

According to their binding energy values component peak *D* was assigned to the carbonyl carbon atoms of quinone-like C=O groups and component peak *E* to the carbonyl carbon atoms of carboxylic acid groups (HO–C=O) and their corresponding carboxylates ($^{\ominus}$O–C=O $\leftrightarrow$ O=C–O$^{\ominus}$). Taking into consideration the fact that oxygen is also bonded in the sulfonate groups (–$SO_3^{\ominus}$) of the polyaniline dispersant, the accounting of the

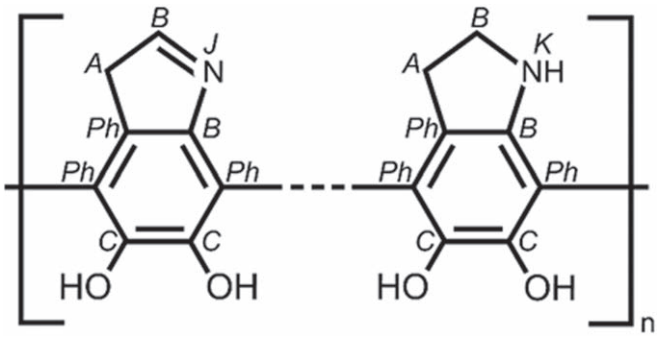

Figure 14. Cut out of the presumed chemical structure of the PDA polymer. Letters denote the assignment of the carbon and nitrogen atoms to the component peaks separated in the high-resolution C 1s and N 1s spectra (figures 13(b) and (c)).

Table 5. Relative contents of nitrogen and oxygen on the surface of differently produced eeG layers. The elemental ratios [N]:[C] and [O]:[C] were determined by means of XPS.

	[N]:[C]	[O]:[C]
Pristine eeG layer	0.02	0.188
DA applied in dispersion	0.049	0.177
DA applied in dispersion, rinsed (approach 3)	0.043	0.184
PDA applied on eeG layers	0.1	0.27
PDA applied on eeG layers, rinsed (approach 2)	0.103	0.289

oxygen-containing functional groups in the C 1s spectrum is in excellent agreement with the ratio for organically bonded oxygen atoms [O]:$[C]_{org}$ ratio of 0.152 which was determined from the wide-scan spectrum.

Component peak *B* appeared from C–N bonds, which were constituents of the dispersant. Its intensity is twice the [N]:[C] ratio, which is confirmed by the chemical structure of the polyaniline chain, C–NH–C and C=N–C ↔ C–N=C. The N 1s spectrum recorded from the sprayed eeG film clearly shows the presence of two differently bonded nitrogen atoms to which component peaks *K* and *L* have been assigned in figure 13 at the right column. According to its binding energy value of 399.27 eV component peak *K* shows the amino groups of the polyaniline dispersant C–NH–C and C=N–C ↔ C–N=C. Component peak *L* at 401.34 eV represents protonated nitrogen species $C–N^{\oplus}H_2–C$. The high degree of protonation resulted from the presence of sulfonic acid groups, which were fully dissociated in the aqueous eeG dispersion ($–SO_3H + H_2O \rightarrow –SO_3^{\ominus} + H_3O^{\oplus}$).

As expected the application of DA increased the [N]:[C] as well as [O]:[C] ratios. However, while the polymerization of DA monomers on the suspended eeG particle surfaces doubled the relative nitrogen content compared to the pristine eeG sample, the application of DA and its polymerization on the sprayed eeG layers increased five times, table 5.

During the polymerization of DA on prepared eeG layers an excellently adhering PDA film was formed. The adhesion of PDA also took place on the surfaces of dispersed eeG colloidal particles.

When the dispersion was kept stable, it was possible to deposit layers from the PDA-coated eeG sheet or particle by spray-coating. Rinsing with 100 ml of water did not induce in washing off the PDA, which is confirmed by the constancy in the surface composition of the differently prepared samples. Compared to the shape of the C 1s spectrum of the pristine eeG sample, the C 1s spectra recorded from the eeG samples carrying surface-polymerized PDA shows a steady tailing that includes the formerly observed second peak maximum, (figure 13(b)) in the middle column). The reason for this is the increase of the nitrogen content and the associated increase in the intensity of component peak *B*. The presence of considerable amounts of saturated hydrocarbons required the introduction of an additional component peak *A* at 285.00 eV.

Nevertheless, the shape of the C 1s spectrum can be considered as a assimilation of photoelectrons coming from the eeG and PDA. Under no circumstances did it correspond to the shape, which is expected for a thick and closed PDA layer. [21]

One was found in the C 1s spectra recorded from eeG layers on which PDA was deposited as a polymer, figure 13(c) middle column. Compared to the component peak *Gr* the main component peak *Ph* was slightly shifted to 284.49 eV. It resulted from the sp^2-hybridized carbon atoms of the phenyl rings, which do not have heteroatoms as binding partners, as shown in figure 14. The origin of the corresponded *shake-up* peaks was

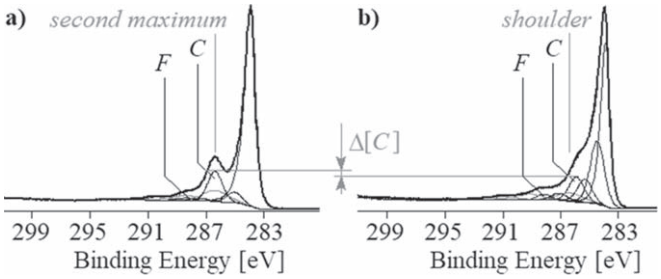

Figure 15. C 1s high-resolution XPS spectra recorded from a spray-coated film made from pristine eeG (a), and a spray-coated film made from eeG with DA polymerized in suspension (b).

explained above. Photoelectrons escaped from the carbon atoms of the phenolic C–OH contributed to component peak *C* at 286.35 eV. Quinone-like groups (C=O), which remain from the oxidative polymerization of the DA monomers were analyzed as component peak *D* at 287.27 eV. Component peak *B* at 285.45 eV resulted from carbon–nitrogen bonds. Its intensity equals the twice of the [N]:[C] ratios determined from the corresponding wide-scan spectrum. According to the structural formula of the PDA (figure 14) the number of carbon atoms carrying phenolic OH groups like C–OH should equal the number of carbon atoms bonded to nitrogen. Since some of the phenolic groups were present in their oxidized form, namely as quinone-like groups (C=O) the sum [*C*] + [*D*] had to equal [*B*]. The N 1s spectrum recorded from eeG samples with a thick and closed PDA layer was completely different to that the one, which was recorded from the pristine eeG sample, seen in figure 13(c) in the right column. The intensity of component peak *L*, which is 401.66 eV, showing protonated amino groups appeared much smaller.

Component peak *K* with 399.91 eV having the highest intensity shows cyclic secondary amino groups (C–NH–C), such as the pyrrolidine structures in figure 14 on the right side [61]. The unusually small binding energy value of the third component peak *J* with 398.44 eV can be explained by high electron densities localized at the concerned nitrogen atoms. These are characteristics of the cyclic imide nitrogen atoms (C–N=C) vividly shown in figure 14 on the left side.

The N 1s spectrum recorded from the eeG sample endowed with surface-polymerized DA polymer ensured that the surface of the eeG sheets and particles was not fully covered by the PDA molecules. Its shape is not much different from that found at pristine eeG which can be found in figure 13(b) in the right column. The intense component peak *L* at 401.82 eV shows protonated amino groups, most of which come from the polyaniline dispersant. However, in contrast to the N 1s spectrum of the pristine eeG sample (figure 13(a)) in the right column), the peak component *J* is evident at 398.8 eV.

The mechanism of the polymerization of DA is not yet fully understood. However, it is indisputable that the polymerization of the DA molecules requires the aid of an oxidizing agent, which is reduced during the polymerization process. Since, the polymerization of DA was carried out in aqueous solutions, which were free of dissolved oxygen, it can be assumed that the oxidizing agent is provided by the pristine eeG material. Pristine eeG particle surface is decorated with a variety of oxygen-carrying functional groups, figure 13(a). The comparison of the C 1s spectra in figure 15 shows that the second maximum in the C 1s spectrum of pristine eeG disappears after the application of PDA on the eeG particle surface. The difference between the two-component peaks C (Δ[C]) appears very small. However, it must be considered that the PDA molecules are intrinsically endowed with carbon-bonded OH groups, whose C 1s photoelectrons contributed to the component peak C. As mentioned above, in the PDA molecule the number of carbon atoms bonded to oxygen equals the number of carbon atoms bonded to nitrogen as shown in figure 14.

From the comparison of the intense components peak B and C in figure 15 we can draw the conclusion that the majority of the photoelectrons counted as component peak C originates from the phenolic OH groups of the PDA molecules. These findings clearly showed that the OH groups on the eeG sheets and particle surface acted as an oxidizing agent during the polymerization of the DA molecules; consequently, they were reduced. Of course, it would be desirable if the carboxylic acid groups were also reduced. This could be a contribution to the repair of eeG graphite-like lattices. However, the presence of component peak F in the C 1s spectrum of the PDA-coated eeG sheets and particles indicated that carboxylic acid groups were kept stable and were not involved in the oxidative polymerization of the DA molecules.

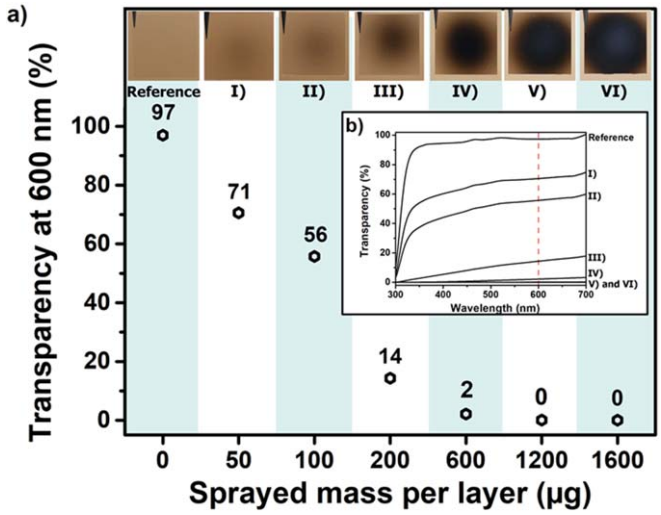

Figure 16. UV/VIS-Measurement of reference (glass) and spray-coated eeG layers with increasing mass per layer from I to VI.

3.7. Transparency of spray-coated eeG layers

Since an electrically conductive material can be contacted and heated not only in the ring structure but also in any other form, eeG layers were spray-coated in order to demonstrate their applicability as transparent and electrically conductive layers.

UV/Vis measurements were performed on the eeG layers to investigate the spectral properties in wavelength range depending upon the sprayed eeG quantity. According to the resulting masses in table 1, figure 16(a) demonstrates the transparency of eeG layers obtained at 600 nm. Figure 16(b) shows the UV/Vis spectra in the wavelength length from 300–700 nm. The respective, roman numbered photographs of eeG layers are also shown, see figure 16(a).

The sample *I* achieved the highest transparency of 71% with approx. 50 μg of sprayed eeG mass. Compared to the reference, the transparency decreased by 26%. Whereas, sample *II* exhibits the transparency of 55.7% with double the deposited eeG mass, sample *III* shows the transparency of 14.3% and from sample *IV* to *VI* a decrease of transparency from 2.1% to 0% was recorded. The measured transparencies can be compared with other reports by Vasanthi *et al* [62], who described spray pyrolyzed multi-layers of exfoliated graphene, Shi *et al* [63] reported spray-coated thin-films of reduced graphene oxide (rGO) at 550 nm.

In figure 16 *I* to *VI*, it is also observed, that the layers show local transparency differences. Edges, e.g. in sample *III*, are visually more translucent than the centre. The mass of sprayed eeG can be approximated by the AoI, but the spatial expansion of the sprayed density follows a Gaussian distribution [42], whose size depends on spray-pressure, dispersion viscosity and working distance [64]. Since a circular AoI of 3 cm diameter was assumed in section 3.1, the disadvantages of a static spraying process become clear.

3.8. Proof of principle of Joule-Heating of eeG layers

Specific material properties like electrical or thermal conductivity and the ability of heat generation are of great importance for applications like thin film heaters or thin films that have suitable heat transfer properties. An efficient way to generate and dissipate heat is crucial for using such materials, e.g. in aircraft windscreens or in smart electrical devices [65]. In order to analyze heating properties, each eeG layer was separately contacted and impinged with an electrical potential. Joule-Heating properties, heat transfer coefficient α and sheet resistance have been verified.

All eeG layers, except the one which was spray-coated with 50 μg eeG and shows the highest transparency, could be heated with the applied currents. The eeG layer with 100 μg eeG could be heated by 0.8 K to 24.8 °C at a voltage of 30 V after 2 min, as shown in figure 17(a). Following this time interval, the heated layer reached an equilibrium or so-called steady-state temperature [66] where no further heating occurred due to an equilibrium between heat generation and dissipation. This is seen in figure 17(b), where the heating rate flattens to 0 K min^{-1} after 2 min. The IR-images on the right side of figures 17(a) and (b) show the temperature rise from 24 °C to 24.8 °C (images *I* to *IV*). The heating area appears in light red. In figures 17(c) and (d), the Joule-Heating of the eeG layer with the highest amount of eeG mass, 1600 μg, is shown. From a voltage of 5 V, heating of approx. 10 K could be achieved with this eeG layer. An increase in voltage is accompanied by larger heat changes than with the eeG layer with 100 μg spray-coating mass. The highest temperature difference of 71 K was achieved at a voltage of 20 V after 30 min. The IR-images on the right side of figures 17(c) and (d) (indicated by roman numbers *I* to

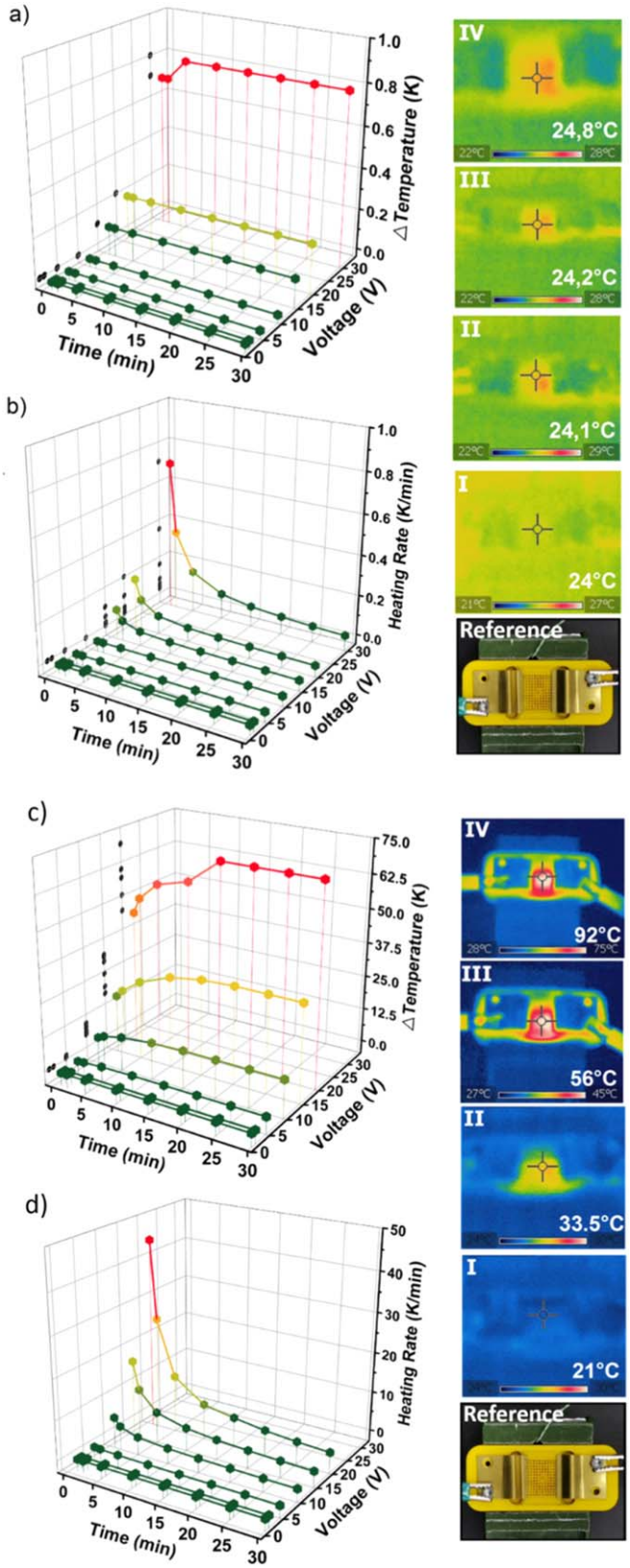

Figure 17. Evaluation of a heating ability with 100 μg spray-coated eeG, (a) calculated temperature difference ΔT between steady state and starting temperature, (b) Heating rate of the examined eeG layer and vice versa for 1600 μg spray-coated eeG in (c) and (d).

IV) show the heating from 21 °C up to 92 °C. To avoid the risk of damage to sample and measuring device, no measurements were carried out at 30 V.

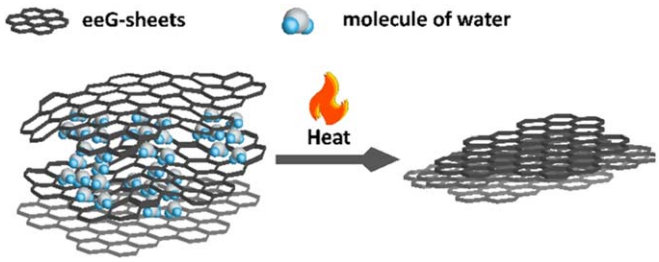

Figure 18. Schematic drawing of eeG-sheets with intercalated water and reduction of eeG-sheet distance due to temperature increase.

The sample with 100 μg eeG mass spray-coated reached the steady state temperature after 2 min. In contrast, the eeG layer with 1600 μg spray-coated eeG mass needed 15 min. It can be assumed that reaching the steady-state-temperature at the same electrical voltage takes longer with increasing sprayed eeG mass.

4. Discussion

Conductive materials, which combine excellent physical [4, 67], chemical [68] and electrical [7, 19, 69] properties, are of great demand in research and industry. Exfoliated graphene [70] is such a promising material. The challenge of producing graphene in large quantities apart from the laboratory scale still remains today, as described by Yang, Lohe or Asli *et al* [19, 27, 71]. These authors developed a preparation procedure for electrochemically exfoliated graphene (eeG) dispersions, which allow an easy application by spray-coating. This makes it possible to produce transparent and at the same time electrically conductive eeG layers. Nevertheless, in our study, such spray-coated layers of eeG showed insufficient material characteristics. Therefore, methods for modification of eeG layers were developed, which can improve the spray-coated material in terms of electrical conductivity.

4.1. Tuning material properties via a bio-inspired modification

Structural changes of manually spray-coated eeG layers through post-treatments were aimed to improve the electrical conductivity towards the extent of modified graphene oxides [30, 32] or the manufacturer's specifications [44]. Two different PDA-based treatments of eeG have been performed and led to sudden increase of electrical conductivity of the treated layers.

By modifying the sprayed eeG/DA dispersion, enormous improvements in the relative changes in electrical conductivity were achieved. The reasons will be discussed in the following sections.

4.1.1. Loss of layer thickness

The losses in layer thickness are evident after the respective thermal annealing and PDA treatments. A reduction of the layer thickness while maintaining the same object geometry influences the calculated electrical conductivity at the same measured resistance.

Three scenarios may lead to a loss of layer thickness. One is the material removal of eeG or densification. The second is the sinking of eeG into the underlying PC layer due to horizontal alignment of sample and annealing driven PC surface softening. The third case is based on a densification of the eeG layer, either by vaporizing the intercalating solvent molecules, compressing the eeG on addition of PDA due to its adhesive properties or shrinkage of PDA as an impact of polymerization.

The exfoliating procedure to form eeG led to the presence of sulfonic groups as shown by XPS [27]. This results in a good dispersibility of the eeG in water. As described by Buddrus *et al* [72], sulfonation converts aromatic compounds into a hydrophilic compound. Therefore, it can be assumed that before spray-coating and despite dilution with ethanol, individual water molecules were enriched at the sulfone groups. As reported by Kieu [73], water molecules accumulate in the curvatures of the planar lattices of the eeG. These curvatures are caused by the presence of hydroxyl groups on the graphene lattice, as described by Schniepp *et al* [74]. As a result, the overlapping of the eeG sheets and particles sometimes causes water molecules and steric barriers of the eeG lattice to overlap. By annealing at 100°C, intercalated water condensates and reacts, as described by Acik *et al* [53], to ketone and ester carbonyl groups. This causes the individual curvatures to collapse, resulting in layer thickness shrinkage and a denser packaging. This is shown schematically in figure 18.

As a result, the annealing of the eeG RS removes enriched water molecules and steric barriers, which leads to the collapse of the layers and a better alignment due to self-assembly of the eeG sheets and particles. This also has the effect on reducing the electrical resistance, as the number of contact points of the eeG sheets or particles

increases, more direct conduction paths for the electrons are available, and highly resistive substances are removed.

The marginal reduction in layer thickness during annealing can be described with the theories just mentioned. However, the observed changes in the material properties during the treatment with PDA and producing eeG/DA RS from an eeG/DA dispersion could exceed the previous changes by annealing. In the coming section, the reasons for this will be explained.

4.1.2. Tailoring the electrical properties of eeG RS

During the spray process, eeG sheets and particles were deposited in randomly disordered aggregates. Residues of the dispersant fill free spaces between the sheets. The resistance of such layers is high because the moving charge carriers have to pass though large number of interfaces. If the dispersant is removed during the drying process, the eeG sheets form a *house of cards* structure. Similar to a *house of cards* built by playing cards, the originally formed structure is mechanically instable. It can collapse, resulting in a denser but still disordered layer (heat applied to accelerate the evaporation of the dispersant may support the spatial organization and ordering of the sheets). Higher amounts of eeG per area increase the tendency to collapse and form a layer with a compacted structure. The increased number of contacts between the eeG sheets increases the electrical conductivity and decreases the resistance. However, the maximum electrical conductivity of the eeG layers cannot be achieved in this way. As can be seen in the C 1s spectrum recorded from a spray-coated film made from pristine eeG (figure 13(a)) the eeG sheets contain numerous OH functionalities (component peak C). From *ab-initio* calculations it is known that OH groups bend the graphene sheets so that they do not form planar sheets [21]. As a result, the overlapped integrals of the wave functions of the π orbitals cannot reach a maximum volume. This limits the maximum space in which p_z electrons are allowed to move.

In this study, we combined eeG suspensions, which were stabilized by the electrically conductive PANi with DA. DA was applied to an established eeG RS and reductions in the layer thicknesses were measured after rinsing and annealing. The rinsing process is not responsible for the reduction of the layer thickness by a simple removal of material. This is shown by the absolute and relative values of the mean layer thickness, which lie between 88 to 64 nm and 83 to 86%. It is evident that the electrical resistance decreases with increasing rinsing volume in addition to the decreasing layer thickness. For the PDA coating without rinsing, the mean electrical resistance decreased by 6% compared to the initial mean electrical resistance. The mean electrical resistance decreased by 13 and 15% for the samples which were rinsed with water.

The decrease in layer thickness is affected by the PDA coating and the subsequent annealing. Starting with the coating process, it is assumed that the surface morphology, curvatures due to defects in the graphene lattice, and/or steric barriers (hydroxy groups) [74, 75], the associated accumulation of water molecules [73], as well as the dynamic accumulation of PDA in the bath during swiveling led to losses of eeG. This assumes a decrease in friction between the individual, stacked eeG sheets and particles, similar to the report of Cho *et al* [76]. In addition, steric obstacles caused by defects and the embedded water molecules create a supposedly higher layer. It is assumed that by swiveling in the PDA solution, enriching PDAs are loosened and thereby detach the adherent eeG particles. This loss of sprayed-on eeG leads to a reduction in the layer thickness. Assuming the eeG loss, the electrical resistance should increase. This is based on the findings in section 3.3, because lower the sprayed eeG mass, higher the measured electrical resistance of untreated eeG RS. Described causality from section 3.3 could be refuted with the measurements from section 3.4.3. With comparable layer thickness the pristine-eeG RS achieves a higher electrical resistance of about 51 kΩ and a lower electrical conductivity of 8 kS m^{-1} compared to the PDA-modified eeG RS, which had an electrical resistance of approximately 4.5 kΩ and an electrical power of 50 kS m^{-1}. Nevertheless, a small reduction of the layer thickness could be achieved compared to the eeG/DA modification.

This apparent contradiction can be justified as follows. The remaining eeG particles present get collapsed after annealing. Intercalated water molecules condensed or reacted with other defects in the eeG lattice. Furthermore, the PDA top layer compressed the eeG RS, since the solution from the bath and rinsing process was also removed during the annealing. This leads to a homogeneous polymeric top layer, which shows internal mechanical tensions due to drying [77, 78] which is transferred to the eeG RS and, as described by Georgakilas *et al* [79], and results in better electrical conductivity.

The second aspect is the reduction of the eeG RS by the PDA formation. It is apparent that the additional rinsing with water has a positive effect on the reduction of electrical resistance. As discussed in section 3.8, the rinsing process did not detach a PDA from the surface. Furthermore, table 5 shows that after rinsing, the ratio of [O]:[C] and [N]:[C] on the measured surface increased. This is an indication of an increased reduction compared to the unrinsed sample. The fact that the PDA does not contribute to better electrical conductivity was shown by the work of Coskun *et al* [80] and Silva *et al* [21]. Despite the loss of eeG, lower electrical resistance and therefore better electrical conductivity could be achieved. Thus, the improvements in electrical material properties are due to the physical and chemical influence of the eeG RS.

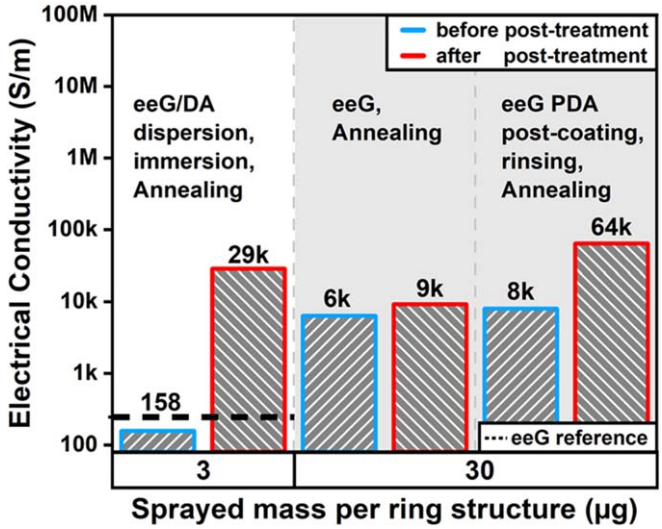

Figure 19. Electrical Conductivity of sprayed-coated pristine eeG (black dotted line); eeG/DA dispersion for 3 μg per structure each, and 30 μg eeG within PDA post-coating (for each sample, after spray-coating means 'before post-treatment' and after Annealing means 'after post treatment').

The layer formation in presence of DA is accompanied by the partial reduction of the pristine eeG, because the pristine eeG acts as an oxidizing agent for the oxidative polymerization of DA to PDA, as shown e.g. in [21]. As can be seen in figure 15(b) the reduction reaction preferably removes OH groups from the eeG sheets and converts them into a more planar structure [21]. The arrangement of the sheets is supported by mechanical stresses which are initiated during the polymerization of DA as a result of the volume shrinkage at the time of formation of the PDA macromolecules. The remaining carboxylic acid groups (component peak *F* in figure 15(b)) localized at the edges of the eeG sheets do not disturb the formation of planar sheets. Orbitals of the p_z electrons, which are perpendicularly aligned with the eeG sheet plane, overlap maximally. Each linear combination of the wave functions of two adjacent p_z electrons results in one lower-energy π molecule orbital and one higher-energy, anti-bonding π^* molecule orbital. The spatial proximity of overlapping orbitals leads to conjugation and a quasi-continuum—a band—where all involved p_z electrons can freely move. Due to the plane structure of the reduced eeG sheets, both the degree of conjugation is superlative. Additionally, contact between different eeG sheets can be closer to plane geometry. The pristine eeG sheets deposited in layers, which were treated with DA, were reduced and coated only in the regions where they come into contact with the DA molecules. The PDA polymer forms a layer concealing the smoothed and mechanically ordered individual eeG sheets (figure 13(c)).

The in-situ graphene modification with dopamine hydrochloride (DA) has been frequently reported [30, 81–83]. In this work, the eeG/DA dispersion was sprayed to develop eeG/DA RS. This part is an extension of the previously published work of Xu *et al* [84]. They created a sprayed membrane layer of graphene in the presence of PDA. Here we consider the effects of further post-treatments like rinsing, immersion, or annealing in relation to the material properties of eeG layers.

The electrical resistance of the modified eeG/DA RS have been tested after spraying and again before annealing. It turned out that the resistances were higher than those of pristine, sprayed 6 ml of 0.25 mg mL^{-1} eeG (30 μg solid content). This is due to the mixing with 2 g/l DA. As a result of an even and homogeneous distribution of the DA molecules, 11% solid content of the eeG was sprayed. The less quantity of eeG sprayed in a 6 ml spray-volume of eeG/DA dispersion compared to the 6 ml of spray-coated eeG with and the resulting electrical resistances from eeG/DA RS are plausible to the values given in section 3.3. This is illustrated in figure 19.

The sudden change in electrical resistance after rinsing and annealing shows the potential of this PDA modification. This is due to the intercalation of the PDA between the eeG layers, the oxidative polymerization from the DA to the PDA, the rinsing processes and the subsequent annealing. The morphological changes shown in section 3.5 in figures 12(e) to (h) remain difficult to interpret. The correlation of the mentioned parameters will be discussed now:

With approx. 7 kΩ as eeG/DA RS resistances, this modification shows a better reduction of the electrical resistance compared to the eightfold sprayed eeG amount coated with PDA. Another detail in the eeG/DA modification is the difference in the analyzed layer thicknesses. While a layer thickness of about 260 nm was achieved when rinsed with 100 ml water, the layer thickness decreased to about 80nm when immersed for

120 min in water. This indicates that material is detached from the deposited layer. The values of the layer thickness of the eeG/DA RS rinsed with 100 ml water illustrates high standard deviation. This can be explained by the inhomogeneous particulate morphology described in section 3.7. The SEM images are similar to those found in the literature. Xie [57] and Xu *et al* [84] showed comparable structures of GO and PDA modified GO. As shown in figures 12(e) to (h), ridge-like structures with additional valleys can be seen. Xie *et al* [57] mention wrinkled graphene particles, which influence the surface roughness. This wrinkle, called the ridge, was also investigated by Kwak *et al* [85]. They found that these defects prevent the oxidation of graphene. This supports the hypothesis that the ridges are unoxidized eeG and the valleys are bulges of the former DA particles that polymerized during post-treatment. This modification improved electrical conductivity noticeably making such layers useful for different heating applications.

Two PDA modification processes have been compared and the potential for further property tuning or customization was presented. For the modification of the PDA coating, the highest electrical conductivity of 64 kS m^{-1} was achieved for the combination with a 20 ml water rinse and 1-hour annealing. Compared to other reported electrical conductivities such as Yang *et al* [12] with 87.1 kS m^{-1} (CVD deposition of graphene), Ma *et al* [55] with 66 kS m^{-1} (modified graphene-based-fiber) or the TDS with >40 kS m^{-1}, the achieved electrical conductivity can be optimized with the applied processes and is therefore competitive. The second modification, the spay-coating of an eeG/DA dispersion and its post-treatment, revealed the highest relative improvement in electrical conductivity of all comparable eeG RS.

Further quantitative experiments have to be performed to demonstrate how much eeG or PDA detaches from the eeG layer or RS and to expand the understanding of intercalating substances, layer collapse and electrical paths in PDA coated graphene.

5. Conclusion

In this work, we investigated material properties of electrochemically exfoliated graphene (eeG), their alteration by using different bio-inspired modifications, and the eeG deposition based on a spray-coating process. The bio-inspired poly(dopamine) (PDA) was applied as a subsequent coating and also sprayed from an eeG/dopamine-hydrochloride (DA) dispersion. Also, the deposition of an eeG/DA dispersion was followed by in-situ polymerization of PDA and post-treatment. The coated or in-situ polymerized PDA was supposed to mechanically stabilize the sprayed eeG structure and reduce the content of oxidized functional groups in eeG to influence the final electrical properties. The PDA coating with additional post-treatment using water and annealing was useful to increase electrical conductivity of the eeG structure as the highest achieved value is 64 kS m^{-1}. This is 16-times higher than the comparable electrical conductivity of 3.9 kS m^{-1} from the similar sized, in layer thickness, spray-coated pristine eeG-RS in section 3.3. The effect is reflected in the electrical conductivity values before, 8 kS m^{-1}, and after, 64 kS m^{-1}, this kind of modification which indicates an increase in electrical conductivity about 800%. The deposition of an eeG/DA dispersion and post-treatment let the electrical conductivity skyrocket from 158 S m^{-1} to 29 kS m^{-1}. Compared with similar- sized layer thickness eeG-structures this value is lower than a PDA-coated and post-treated sample which is shown in figure 9(b) but about 7-times higher than a spray-coated pristine eeG-RS. The effect of this approach let the electrical conductivity increase by 18000%.

With the possibility to tailor the electrical properties of sprayed eeG can be positively influenced e.g. the performance of applications like the described Joule-Heating. Due to an improved electrical conductivity, sprayed eeG structures can be heated with lower currents. The main structural influences of the PDA based deposition methods are on the one hand based on curing of the graphene sheets and the associated reduction of the electrical resistance. On the other hand, the contact between the eeG sheets is reduced by the formed PDA molecules. With a fundamental understanding of this interplay, the electrical properties of the eeG layers can be tailored for a particular application with a defined amount of DA and a known size of the eeG sheets. The impact of both effects on the electrical properties suggests that for larger eeG sheet dimensions the use of eeG/DA dispersion process is advantageous in cases where a maximum reduction in electrical resistance is desired. In contrast, for smaller sheet dimensions the DA post-treatment method seems to be more suitable. It requires further reasearches to provide new insights and fully understand the phenomenon of PDA and the achieved eeG material property changes and their possible ranges of variation.

Acknowledgments

This research work was funded by the Federal Ministry of Education and Research (BMBF) project no. 01DS19024.

Special thanks to Mathias Ullrich and Dr Wolfgang Jenschke, both from Leibniz Institute of Polymer Research Dresden, Germany, who designed the technical concept and built the resistance measurement and Joule-Heating units.

Thanks to Cláudia Silva for her initiation of the work, starting the first experiments and building the foundation for this study.

Thanks to Adrian Romani Vazquez (Chair of Molecular Functional Materials) and Alex Than (Dresden Center for Nanoanalysis (DCN)) from Technische Universiät Dresden, Germany for recording SEM images of the pristine eeG.

ORCID iDs

Petra Pötschke https://orcid.org/0000-0001-6392-7880
Andreas Janke https://orcid.org/0000-0002-9125-4131
Cordelia Zimmerer https://orcid.org/0000-0001-9829-5238

References

[1] Boehm H P, Clauss A, Fischer G O and Hofmann U 1962 Das Adsorptionsverhalten sehr dünner Kohlenstoff-Folien *Z. Anorg. Allg. Chem.* **316** 119–27
[2] Novoselov K S, Geim A K, Morozov S V, Jiang D, Zhang Y, Dubonos S V, Grigorieva I V and Firsov A A 2004 Electric field effect in atomically thin carbon films *Science* **306** 666–9
[3] Boehm H-P 2010 Graphen - wie eine Laborkuriosität plötzlich äußerst interessant wurde *Angew. Chem.* **122** 9520–3
[4] Akinwande D *et al* 2017 A review on mechanics and mechanical properties of 2D materials—Graphene and beyond *Extreme Mechanics Letters* **13** 42–77
[5] Zhang Y, Heo Y-J, Son Y-R, In I, An K-H, Kim B-J and Park S-J 2019 Recent advanced thermal interfacial materials: a review of conducting mechanisms and parameters of carbon materials *Carbon* **142** 445–60
[6] Wallace P R 1947 The band theory of graphite *Phys. Rev.* **71** 622–34
[7] Kim M-S, Kim M, Son S, Cho S-Y, Lee S, Won D-K, Ryu J, Bae I, Kim H-M and Kim K-B 2020 Sheet resistance analysis of interface-engineered multilayer graphene: mobility versus sheet carrier concentration *ACS Applied Materials & Interfaces* **12** 30932–40
[8] Crossno J *et al* 2016 Observation of the Dirac fluid and the breakdown of the Wiedemann-Franz law in graphene *Science* **351** 1058–61
[9] Lee C, Wei X, Kysar J W and Hone J 2008 Measurement of the elastic properties and intrinsic strength of monolayer graphene *Science* **321** 385–8
[10] Li Y and Chopra N 2014 Progress in large-scale production of graphene. Part 1: chemical methods *JOM* **67** 34–43
[11] Li D 2019 Market analysis for advanced materials 2020 *International Journal of Advancements in Technology* https://longdom.org/open-access/market-analysis-for-advanced-materials-2020.pdf
[12] Yang H, Cao Y, He J, Zhang Y, Jin B, Sun J-L, Wang Y and Zhao Z 2017 Highly conductive free-standing reduced graphene oxide thin films for fast photoelectric devices *Carbon* **115** 561–70
[13] Li C, Xu Y-T, Zhao B, Jiang L, Chen S-G, Xu J-B, Fu X-Z, Sun R and Wong C-P 2015 Flexible graphene electrothermal films made from electrochemically exfoliated graphite *J. Mater. Sci.* **51** 1043–51
[14] Zhang Y, Liu H, Tan L, Zhang Y, Jeppson K, Wei B and Liu J 2019 Properties of undoped few-layer graphene-based transparent heaters *Materials* **13** 104
[15] Yang J-W, Yu Z-Y, Cheng S-J, Chung J H Y, Liu X, Wu C-Y, Lin S-F and Chen G-Y 2020 Graphene oxide–based nanomaterials: an insight into retinal prosthesis *Int. J. Mol. Sci.* **21** 2957
[16] Coroş M, Pogăcean F, Măgeruşan L, Socaci C and Pruneanu S 2019 A brief overview on synthesis and applications of graphene and graphene-based nanomaterials *Frontiers Mater. Sci.* **13** 23–32
[17] Tour J M 2013 Top-Down versus bottom-up fabrication of graphene-based electronics *Chem. Mater.* **26** 163–71
[18] Liu F, Wang C, Sui X, Riaz M A, Xu M, Wei L and Chen Y 2019 Synthesis of graphene materials by electrochemical exfoliation: recent progress and future potential *Carbon Energy* **1** 173–99
[19] Yang S, Lohe M R, Müllen K and Xinliang F 2016 New-generation graphene from electrochemical approaches: production and applications *Adv. Mater.* **28** 6213–21
[20] Gnanaseelan M, Samanta S, Pionteck J, Jehnichen D, Simon F, Pötschke P and Voit B 2019 Vanadium salt assisted solvothermal reduction of graphene oxide and the thermoelectric characterisation of the reduced graphene oxide in bulk and as composite *Mater. Chem. Phys.* **229** 319–29
[21] Silva C, Simon F, Friedel P, Pötschke P and Zimmerer C 2019 Elucidating the chemistry behind the reduction of graphene oxide using a green approach with polydopamine *Nanomaterials* **9** 902
[22] Li B, Hu N, Su Y, Yang Z, Shao F, Li G, Zhang C and Zhang Y 2019 Direct Inkjet Printing of Aqueous Inks to Flexible All-Solid-State Graphene Hybrid Micro-Supercapacitors *ACS Applied Materials & Interfaces* **11** 46044–53
[23] Ng L W T, Zhu X, Hu G, Macadam N, Um D, Wu T-C, Moal F L, Jones C and Hasan T 2019 Conformal printing of graphene for single- and multilayered devices onto arbitrarily shaped 3D surfaces *Adv. Funct. Mater.* **29** 1807933
[24] Fotovvati B, Namdari N and Dehghanghadikolaei A 2019 On coating techniques for surface protection: a review *Journal of Manufacturing and Materials Processing* **3** 28
[25] Li D, Müller M B, Gilje S, Kaner R B and Wallace G G 2008 Processable aqueous dispersions of graphene nanosheets *Nat. Nanotechnol.* **3** 101–5
[26] Wilkinson N J, Smith A A M, Kay R W and Harris R A 2019 A review of aerosol jet printing—a non-traditional hybrid process for micro-manufacturing *The International Journal of Advanced Manufacturing Technology* **105** 4599–619
[27] Lohe M R, Feng X and Nia Shaygan A 2017 *Sixonia Tech GmbH*Verfahren zur Herstellung eines funktionalisierten Halbleiter- oder Leitermaterials und dessen VerwendungPatent DE102017223892A1

[28] Ryu J H, Messersmith P B and Lee H 2018 Polydopamine surface chemistry: a decade of discovery *ACS Applied Materials & Interfaces* **10** 7523–40
[29] Ball V 2018 Polydopamine nanomaterials: recent advances in synthesis methods and applications *Frontiers in Bioengineering and Biotechnology* **6** 109
[30] Cui M, Ren S, Zhao H, Xue Q and Wang L 2018 Polydopamine coated graphene oxide for anticorrosive reinforcement of water-borne epoxy coating *Chem. Eng. J.* **335** 255–66
[31] Luo F, Wu K, Shi J, Du X, Li X, Yang L and Lu M 2017 Green reduction of graphene oxide by polydopamine to a construct flexible film: superior flame retardancy and high thermal conductivity *Journal of Materials Chemistry A* **5** 18542–50
[32] Xu L Q, Yang W J, Neoh K-G, Kang E-T and Fu G D 2010 Dopamine-induced reduction and functionalization of graphene oxide nanosheets *Macromolecules* **43** 8336–9
[33] Miao J, Liu H, Li W and Zhang X 2016 Mussel-inspired polydopamine-functionalized graphene as a conductive adhesion promoter and protective layer for silver nanowire transparent electrodes *Langmuir* **32** 5365–72
[34] Yu X, Walsh J and Wei M 2014 Covalent immobilization of collagen on titanium through polydopamine coating to improve cellular performances of MC3T3-E1 cells *RSC Adv.* **4** 7185
[35] Li S, Zhu J, Yu J, Wang Y and Hu Z 2019 Mussel-inspired polydopamine/polystyrene composites with 3D continuous structure and improved thermal, mechanical, and flame retarding properties *J. Appl. Polym. Sci.* **136** 47740
[36] Qiu X, Kundu C K, Li Z, Li X and Zhang Z 2019 Layer-by-layer-assembled flame-retardant coatings from polydopamine-induced in situ functionalized and reduced graphene oxide *J. Mater. Sci.* **54** 13848–62
[37] Fredi G, Simon F, Sychev D, Melnyk I, Janke A, Scheffler C and Zimmerer C 2020 Bioinspired polydopamine coating as an adhesion enhancer between paraffin microcapsules and an epoxy matrix *ACS Omega* **5** 19639–53
[38] Zimmerer C, Mejia C, Utech T, Arnhold K, Janke A and Wosnitza J 2019 Inductive heating using a high-magnetic-field pulse to initiate chemical reactions to generate composite materials *Polymers* **11** 535
[39] Silva C A, Pötschke P, Simon F, Holzschuh M, Pionteck J, Heinrich G, Wießner S and Zimmerer C 2019 Synthesis and characterization of graphene derivatives for application in magnetic high-field induction heating *AIP Conf. Proc.* **2055** 130006
[40] Novais R M, Simon F, Pötschke P, Villmow T, Covas J A and Paiva M C 2013 Poly (lactic acid) composites with poly (lactic acid)-modified carbon nanotubes *J. Polym. Sci., Part A: Polym. Chem.* **51** 3740–50
[41] Shirley D A 1972 High-resolution x-ray photoemission spectrum of the valence bands of gold *Physical Review B* **5** 4709–14
[42] Scalera L, Mazzon E, Gallina P and Gasparetto A 2017 Airbrush robotic painting system: experimental validation of a colour spray model *Advances in Service and Industrial Robotics* 549–56
[43] Nasim M, Vo Q. T, Mustafi L, Kim B, Lee C S, Chu W-S and Chun D-M 2019 Deposition mechanism of graphene flakes directly from graphite particles in the kinetic spray process studied using molecular dynamics simulation *Comput. Mater. Sci.* **169** 109091 11
[44] Lohe D M R Sixonia Tech GmbH, 'Technical Data Sheet E-Graphene Dispersion G-DISP-H2O-CSO-2'
[45] Nistal A, Garcia E, Coll D P, Prieto C, Belmonte M, Osendi M I and Miranzo P 2018 Low percolation threshold in highly conducting graphene nanoplatelets/glass composite coatings *Carbon* **139** 556–63
[46] Taherian R 2016 Experimental and analytical model for the electrical conductivity of polymer-based nanocomposites *Compos. Sci. Technol.* **123** 17–31
[47] Orts W J, Zanten J H, Wu W-L and Satija K S 1993 Observation of temperature dependent thicknesses in ultrathin polystyrene films on silicon *Phys. Rev. Lett.* **71** 867–70
[48] Kanaya T, Miyazaki T, Watanabe H, Nishida K, Yamano H, Tasaki S and Bucknall D B 2003 Annealing effects on thickness of polystyrene thin films as studied by neutron reflectivity *Polymer* **44** 3769–73
[49] Kobashi K, Villmow T, Andres T and Pötschke P 2008 Liquid sensing of melt-processed poly(lactic acid)/multi-walled carbon nanotube composite films *Sensors Actuators B* **134** 787–95
[50] Reiter G and Napolitano S 2010 Possible origin of thickness-dependent deviations from bulk properties of thin polymer films *J. Polym. Sci., Part B: Polym. Phys.* **48** 2544–7
[51] Frank C W, Rao V, Despotopoulou M M, Pease F W R, Hinsberg W D, Miller R D and Rabolt J F 1996 Structure in thin and ultrathin spin-cast polymer films *Science* **273** 912–5
[52] Yang C, Li Q, Mao W, Wang P and He C 2015 On crystallization of bisphenol-A polycarbonate thin films upon annealing *Phys. Lett. A* **379** 2515–9
[53] Acik M, Mattevi C, Gong C, Lee G, Cho K, Chhowalla M and Chabal Y J 2010 The role of intercalated water in multilayered graphene oxide *ACS Nano* **4** 5861–8
[54] Zhao Z, Guo L, Feng L, Lu H, Xu Y, Wang J, Xiang B and Zou X 2019 Polydopamine functionalized graphene oxide nanocomposites reinforced the corrosion protection and adhesion properties of waterborne polyurethane coatings *Eur. Polym. J.* **120** 109249
[55] Ma T, Gao H-L, Cong H-P, Yao H-B, Wu L, Yu Z-Y, Chen S-M and Yu S-H 2018 A bioinspired interface design for improving the strength and electrical conductivity of graphene-based fibers *Adv. Mater.* **30** 1706435
[56] Geng D, Yang S, Zhang Y, Yang J, Liu J, Li R, Sham T-K, Sun X, Ye S and Knights S 2011 Nitrogen doping effects on the structure of graphene *Appl. Surf. Sci.* **257** 9193–8
[57] Xie J and Spallas J P 2012 Different contrast mechanisms in SEM imaging of graphene *Agil. Technol*
[58] Dimiev A, Kosynkin D V, Sinitskii A, Slesarev A, Sun Z and Tour J M 2011 Layer-by-layer removal of graphene for device patterning *Science* **331** 1168–72
[59] Pinithchaisakula A, Themsirimongkon S, Promsawan N, Weankeaw P, Ounnunkad K and Saipanya S 2016 An investigation of a polydopamine-graphene oxide composite as a support for an anode fuel cell catalyst *Electrocatalysis* **8** 36–45
[60] Li L *et al* 2019 Polydopamine coating promotes early osteogenesis in 3D printing porous Ti6Al4V scaffolds *Annals of Translational Medicine* **7** 240–240
[61] Tripathi B P, Das P, Simon F and Stamm M 2018 Ultralow fouling membranes by surface modification with functional polydopamine *Eur. Polym. J.* **99** 80–9
[62] Vasanthi V, Logu T, Ramakrishnan V, Anitha K and Sethuraman K 2019 Study of electrical conductivity and photoelectric response of liquid phase exfoliated graphene thin film prepared via spray pyrolysis route *Carbon Letters* **30** 417–23
[63] Shi H, Wang C, Sun Z, Zhou Y, Jin K and Yang G 2014 Transparent conductive reduced graphene oxide thin films produced by spray coating *Science China Physics, Mechanics & Astronomy* **58** 1–5
[64] Cassano C L, Georgiev T Z and Fan Z H 2017 Using airbrushes to pattern reagents for microarrays and paper-fluidic devices *Microsystems & Nanoengineering* **3** 1–7
[65] Gupta R, Rao D. M. K, Kiruthika S and Kulkarni G U 2016 Visibly transparent heaters *ACS Applied Materials & Interfaces* **8** 12559–75
[66] Bergman T L, Incropera F P, DeWitt D P and Lavine A S 2011 *Fundamentals of Heat and Mass Transfer* (New York: Wiley)

[67] Iqbal A A, Sakib N, Iqbal K M P A and Nuruzzaman D M 2020 Graphene-based nano-composites and their fabrication, mechanical properties and applications *Materialia* **12** 100815
[68] Tung T T, Alotaibi F, Nine M J, Silva R, Tran N H D, Janowska I and Losic D 2018 Engineering of highly conductive and ultra-thin nitrogen-doped graphene films by combined methods of microwave irradiation, ultrasonic spraying and thermal annealing *Chem. Eng. J.* **338** 764–73
[69] Wang K, Shen L, Song C, Zhang Y and Chen P 2020 The electrical performance and conductive network of reduced graphene oxide-coated ultra-high-molecular-weight polyethylene fibers through electrostatic interaction and covalent bonding *J. Appl. Polym. Sci.* **137** 48946
[70] Novoselov K S, Jiang D, Schedin F, Booth T J, Khotkevich V V, Morozov S V and Geim A K 2005 Two-dimensional atomic crystals *Proc. Natl Acad. Sci.* **102** 10451–3
[71] Asli A E N, Guo J, Lai P L, Montazami R and Hashemi N N 2020 High-yield production of aqueous graphene for electrohydrodynamic drop-on-demand printing of biocompatible conductive patterns *Biosensors* **10** 6
[72] Buddrus J and Schmidt B 2014 *Grundlagen der Organischen Chemie* (Germany: De Gruyter GmbH & Co KG)
[73] Kieu H T, Zhou K and Law A W-K 2019 Surface morphology effect on the evaporation of water on graphene oxide: a molecular dynamics study *Appl. Surf. Sci.* **488** 335–42
[74] Schniepp H C, Li J-L, McAllister M J, Sai H, Herrera-Alonso M, Adamson D H, Prud'homme R K, Car R, Saville D A and Aksay I A 2006 Functionalized single graphene sheets derived from splitting graphite oxide *The Journal of Physical Chemistry B* **110** 8535–9
[75] Shen X, Lin X, Yousefi N, Jia J and Kim J-K 2014 Wrinkling in graphene sheets and graphene oxide papers *Carbon* **66** 84–92
[76] Cho D-H, Wang L, Kim J-S, Lee G-H, Kim E S, Lee S, Lee S Y, Hone J and Lee C 2013 Effect of surface morphology on friction of graphene on various substrates *Nanoscale* **5** 3063
[77] Lei H, Payne J A, McCormick A V, Francis L F, Gerberich W W and Scriven L E 2001 Stress development in drying coatings *J. Appl. Polym. Sci.* **81** 1000–13
[78] Perera D Y 1996 On adhesion and stress in organic coatings *Prog. Org. Coat.* **28** 21–3
[79] Georgakilas V, Koutsioukis A, Petr M, Tucek J and Zboril R 2016 Remarkable enhancement of the electrical conductivity of carbon nanostructured thin films after compression *Nanoscale* **8** 11413–7
[80] Coskun H, Aljabour A, Uiberlacker L, Strobel M, Hild S, Cobet C, Farka D, Stadler P and Sariciftci N S 2018 Chemical vapor deposition - based synthesis of conductive polydopamine thin-films *Thin Solid Films* **645** 320–5
[81] Kanyong P, Krampa F D, Aniweh Y and Awandare G A 2020 Polydopamine-functionalized graphene nanoplatelet smart conducting electrode for bio-sensing applications *Arabian J. Chem.* **13** 1669–77
[82] Ma J, He Y, Zeng G, Li F, Li Y, Xiao J and Yang S 2017 Bio-inspired method to fabricate poly-dopamine/reduced graphene oxide composite membranes for dyes and heavy metal ion removal *Polym. Adv. Technol.* **29** 941–50
[83] Yang X, Niu X, Mo Z, Guo R, Liu N, Zhao P and Liu Z 2019 Electrochemical chiral interface based on the Michael addition/Schiff base reaction of polydopamine functionalized reduced graphene oxide *Electrochim. Acta* **319** 705–15
[84] Xu Y, Wu M, Yu S, Zhao Y, Gao C and Shen J 2019 Ultrathin and stable graphene oxide film via intercalation polymerization of polydopamine for preparation of digital inkjet printing dye *J. Membr. Sci.* **586** 15–22
[85] Kwak J, Jo Y, Park S-D, Kim N Y, Kim S-Y, Shin H-J, Lee Z, Kim S Y and Kwon S-Y 2017 Oxidation behavior of graphene-coated copper at intrinsic graphene defects of different origins *Nat. Commun.* **8** 1–12